

Design and Evaluation of MIMO Terminal Antennas with Adaptive Matching in Realistic User Scenarios

Ehsan Foroozanfard

November 15, 2012

Abstract

The Long Term Evolution (LTE) standard for wireless communication devices requires the use of multiple-input multiple-output (MIMO) technology in user terminals. However, since mobile phones are small in size, the design of multi-antennas is challenging. Moreover, the influence of user proximity and propagation environment must also be considered in the design. In addition, due to the non-stationary nature of the user and propagation channel, the multi-antennas must adapt to changes in order to achieve optimal performance. The major aim of the thesis project is to evaluate and compare the performance of three multi-antenna prototypes equipped with adaptive impedance matching networks. We estimate the capacity gain from employing this adaptive method in realistic scenarios. The user scenarios are achieved with a homogeneous hand model whose posture can be conveniently manipulated to emulate different hand grips. The first phase of the project involved the design of three different dual-band, dual-antenna prototypes for LTE bands 7 and 13. The antenna elements used in the prototypes are planar inverted-F antennas (PIFAs) and slot-monopole antennas. In the second phase, the prototypes were evaluated at the low frequency band in four user scenarios which are: one hand (data mode, talk mode), two hands and free space. Finally, capacity gains from applying adaptive impedance matching were calculated and analysed for the low band. The results show that the first prototype offers the highest capacity improvement at the center frequency (i.e., 27%), obtained for the talk mode scenario. In addition, the mean capacity is improved by 22% over the band of interest.

Acknowledgments

I would like to thank my supervisors Ivaylo Vasilev and Dr. Buon Kiong Lau for their kind support and constructive criticisms through the entire project. And most importantly, many thanks to my family who has always been supportive and believed in me.

Table of Contents

1	Introduction	3
1.1	Background	3
1.2	Objective	3
2	Antenna Design	5
2.1	MIMO antenna overview	5
2.2	Antenna types	6
2.2.1	PIFAs	6
2.2.2	Slot-monopole antenna	6
2.3	Antenna prototypes	7
2.3.1	Prototype I-PIFA center	8
2.3.2	Prototype II-PIFA rotated-center	12
2.3.3	Prototype III-PIFA edge	14
2.4	Measures of performance	15
2.4.1	Efficiency	15
2.4.2	Correlation	16
2.4.3	Radiation Pattern	18
3	User Effect Study	21
3.1	User effect overview	21
3.2	Hand phantoms	22
3.2.1	Models	22
3.2.2	Makehuman models	22
3.3	One-hand scenarios	23
3.3.1	Talk Mode	23
3.3.2	Data Mode	26
3.4	Two-hand scenario	29
4	Adaptive Impedance Matching	33
4.1	Introduction	33

4.2	Principle of Operation	34
4.3	Numerical study	35
4.3.1	Capacity	35
5	Results _____	37
5.1	Prototype I	37
5.1.1	Talk mode	37
5.1.2	Data mode	38
5.1.3	Two hands	39
5.2	Prototype II	40
5.3	Prototype III	41
5.3.1	One hand data mode	41
5.3.2	One hand talk mode	41
5.3.3	Two hands	42
5.4	Prototypes Comparison	43
5.4.1	Over the bandwidth-Two hands	43
5.4.2	Results at the center frequency	45
6	Conclusion _____	47
A	Impedance Matching Results _____	49
A.1	Prototype I	49
A.1.1	Free space	49
A.1.2	One hand data mode	50
A.1.3	One hand talk mode	51
A.1.4	Two hands	52
A.2	Prototype II	53
A.2.1	Free space	53
A.2.2	One hand data mode	54
A.2.3	One hand talk mode	55
A.2.4	Two hands	56
A.3	Prototype III	56
A.3.1	Free space	56
A.3.2	One hand data mode	58
A.3.3	One hand talk mode	59
A.3.4	Two hands	60
	References _____	61

List of Figures

2.1	Geometry of Slot-M antenna	8
2.2	Current distributions of Slot-M antenna	9
2.3	Geometry of the PIFA	10
2.4	Current distributions of PIFA	11
2.5	S parameters for Prototype I in free space	12
2.6	Structure of Prototype II	13
2.7	S parameters for Prototype II in free space	13
2.8	Structure of Prototype III	14
2.9	S parameters for Prototype III in free space	15
2.10	Radiation pattern of Prototype I at 750 MHz	18
2.11	Radiation pattern of Prototype II at 767 MHz	19
2.12	Radiation pattern of Prototype III at 767 MHz	19
3.1	Makehuman software	23
3.2	One hand talk mode scenario	24
3.3	S parameters of Prototype I in talk mode	25
3.4	S parameters of Prototype II in talk mode	25
3.5	S parameters of Prototype III in talk mode	26
3.6	One hand data mode scenario	27
3.7	S parameters of Prototype I in data mode	27
3.8	S parameters of Prototype II in data mode	28
3.9	S parameters of Prototype III in data mode	29
3.10	Two hand (or game mode) scenario	29
3.11	S parameters of Prototype I in game mode	30
3.12	S parameters of Prototype II in game mode	31
3.13	S parameters of Prototype III in game mode	31
4.1	Considered states in Smith chart	33
4.2	Antennas and adaptive impedance matching networks	34

- 5.1 Capacity and efficiency for one hand talk mode (Prototype I) 38
- 5.2 Capacity and efficiency for two hands (Prototype I) 39
- 5.3 Capacity and efficiency for one hand talk mode (Prototype II) 40
- 5.4 Capacity and efficiency for one hand data mode (Prototype III) 41
- 5.5 Capacity and efficiency for one hand talk mode (Prototype III) 42
- 5.6 Capacity and efficiency for two hands (Prototype III) 43
- 5.7 Efficiency for two hands (game mode) 44
- 5.8 Correlation and capacity comparison 44

- A.1 Capacity for Prototype I in free space 49
- A.2 Efficiency and correlation of Prototype I in free space 50
- A.3 Capacity for Prototype I in data mode 50
- A.4 Efficiency and correlation of Prototype I in data mode 51
- A.5 Capacity for Prototype I in talk mode 51
- A.6 Efficiency and correlation of Prototype I in talk mode 52
- A.7 Capacity for Prototype I in game mode 52
- A.8 Efficiency and correlation of Prototype I in game mode 53
- A.9 Capacity for Prototype II in free space 53
- A.10 Efficiency and correlation of Prototype II in free space 54
- A.11 Capacity for Prototype II in data mode 54
- A.12 Efficiency and correlation of Prototype II in data mode 55
- A.13 Capacity for Prototype II in talk mode 55
- A.14 Efficiency and correlation of Prototype II in talk mode 56
- A.15 Capacity for Prototype II in game mode 56
- A.16 Efficiency and correlation of Prototype II in game mode 57
- A.17 Capacity for Prototype III in free space 57
- A.18 Efficiency and correlation of Prototype III in free space 57
- A.19 Capacity for Prototype III in data mode 58
- A.20 Efficiency and correlation of Prototype III in data mode 58
- A.21 Capacity for Prototype III in talk mode 59
- A.22 Efficiency and correlation of Prototype III in talk mode 59
- A.23 Capacity for Prototype III in game mode 60
- A.24 Efficiency and correlation of Prototype III in game mode 60

List of Tables

2.1	Radiation efficiency (free space)	16
2.2	Total efficiency (free space)	16
2.3	Correlation coefficient (free space)	17
5.1	Capacity and correlation at center frequency	45
5.2	Total efficiency of the three prototypes at center frequency .	45

Introduction

1.1 Background

To make radio communication more robust, various diversity techniques are employed in communication systems. These diversity techniques can be in different domains such as time diversity, frequency diversity and spatial diversity. Spatial diversity techniques demand the use of multiple-input multiple-output (MIMO) systems. Moreover, MIMO technology can be used to increase data rate (spatial multiplexing).

The purpose of spatial diversity is to make the transmission more robust. There is no increase in the data rate. This mode uses redundant data on distinct sets of propagation paths. Spatial multiplexing is not intended to make the transmission more robust; rather it increases the data rate. To do this, the data is divided into separate streams; the streams are transmitted independently via separate antennas. Even though MIMO systems have high reliability and high data rate, the design of these systems is more complex compared to conventional single-input single-output (SISO) systems. In the context of terminal application, the user terminal's limitation in size does not give so much freedom in terms of implementation space to antenna designers. In addition, coupling and correlation among the antennas become important considerations for compact multiple antenna terminals.

1.2 Objective

The major aim of the thesis project is to evaluate and compare the performance of three multiple antenna prototypes with adaptive impedance matching networks. We estimate the capacity gains from employing this adaptive method in realistic user scenarios. The user scenarios are achieved with a homogeneous hand model that can be brought to any pose. The

first phase of the project involved the design of three different dual-band dual antennas for LTE bands 7 and 13. The antenna elements used in the prototypes are Planar Inverted-F Antenna (PIFA) and Slot-Monopole. In the second phase, the three prototypes were evaluated in four user scenarios which were: one hand (data mode, talk mode), two hands and free space. The capacity gain results from adaptive impedance matching were calculated in the last phase.

Antenna Design

2.1 MIMO antenna overview

Recent developments in communication systems have increased the need for MIMO antennas, due to the demand for higher spectral efficiency, higher channel capacity, etc. However, designing and implementing multiple antennas in compact terminal devices is challenging, since it involves both practical and fundamental design tradeoffs [1].

Space constraint- This is a very important issue for multiple antenna design in mobile terminals, since it forces antennas to be closely spaced. Consequences will be the high spatial correlation and strong mutual coupling of which the latter reduces the radiated and received power (and influences spatial correlation) and the former reduces spatial degrees of freedom (DoFs) [3].

Bandwidth- To comply with wireless communication standards, antenna designers should consider the co-existence of multiple antennas that cover the same frequency band(s) within a given terminal device [3].

Mobile chassis- Recent studies [1] show that the mobile chassis has significant effects on antenna performance. Based on Characteristic Mode Analysis, the influence of the mobile chassis is found to be the most critical design factor for multiple antenna terminals at frequency bands lower than 1 GHz. Based on the characteristics of ground plane excitation, multiple antennas can be appropriately located on the ground plane to achieve low coupling [1].

In this project, dual-antenna prototypes are enclosed in a volume of $126 \times 66 \times 7.5 \text{ mm}^3$, which corresponds to the size of a typical smart phones today.

The first antenna (port 1) is a dual-band slot-monopole (Slot-M), which has been tuned for LTE-band 13 (from 746 MHz till 787 MHz) and LTE-band 7 (from 2.5 GHz till 2.69 GHz) [8]. Port 2 is a dual-band Planar Inverted-F Antenna (PIFA). More details about these antennas are provided in the following section.

2.2 Antenna types

2.2.1 PIFAs

PIFAs have been extensively used in mobile communication devices, such as mobile phones and laptop computers, as a result of low cost, small size and multi-band properties [5].

The principle behind the PIFA is that, if you assume a half-wavelength patch antenna, the current distribution on the patch is at its peak at the center and goes to zero at the edges (ends), because current has nowhere to flow. On the other hand the voltage distribution is out of phase with the current distribution. It peaks at the edge and it has a zero value at the center. Therefore right at the center of the half-wavelength patch we have zero voltage and maximum current which actually leads to short circuit ($Z = \frac{V}{I}$). As a consequence of that, we do not really need the half section of the patch, so we can make short-circuit at the center and delete half of the patch surface, with the remaining half still maintaining the same current and voltage distributions.

Hence a PIFA is the result of shrinking a patch antenna, as a result it resonates at a quarter-wavelength. The price for reducing the size is a loss in bandwidth.

In this project, a modified dual-band PIFA based on the design in [1] is used. The original design in [1] is for the ground size of $100 \times 40 \text{ mm}^2$ and in this work, the PIFA is retuned for the chassis size of $(126 \times 66 \text{ mm}^2)$. More details about the tuning of the antenna will follow in the antenna prototype section.

2.2.2 Slot-monopole antenna

A slot-monopole antenna can be obtained by cutting out a slot at the edge of the ground plane and leaving it with an open end. The slot length should

be a quarter of the wavelength at the desired frequency of resonance. Slot-monopole antennas have an open end which decreases the size of the antenna and makes it promising for mobile handset applications.

Slot-monopole antennas are derived from half-wavelength slot antennas. The principle behind the half-wavelength slot antenna is that the slot length is much larger than the width, and the entire slot is enclosed in the ground plane. The voltage at the two ends of the slot has to be very close to zero because of small slot width. Therefore we can assume zero voltage at the edges and maximum voltage at the center.

For the current distribution the peak values are at the ends and zero at the center, consequently for radiating antenna we need the current to add up in phase or the voltage to add up in phase. For slot antennas, the current distributions cancel out, though the voltage adds up in phase, so the antenna can radiate. The impedance has the maximum value at the center and minimum value at the edges. Therefore the feed point can be chosen between these points to match the characteristic impedance of the feed cable. Moreover from the duality theory, a slot antenna is the complementary antenna of the dipole, because the dipole is a metal wire surrounded by air, while the slot antenna is an air gap surrounded by ground plane. So the duality principle says that the radiation pattern will be the same in terms of magnitude. Slot-monopole antenna is the modified version of the slot antenna which occupies a smaller space on the mobile chassis.

In this project, a dual-band slot-monopole antenna has been designed based on [1] and [2], and we will refer to it as Slot-M antenna.

2.3 Antenna prototypes

In this section, different combinations of antenna locations are studied to clarify the effect of location on antenna matching and on the isolation between the two antennas.

In all the simulations, the two antennas (Slot-M and PIFA) are integrated onto the same chassis of the dimensions of $126 \times 66 \text{ mm}^2$. The Slot-M antenna is fixed at one short edge, and the PIFA is placed in three different positions (center, rotated center and the other short edge). The design has been modified from [1], which has been done for a smaller ground plane size ($100 \times 40 \text{ mm}^2$). All the simulations have been done with CST Microwave Studio using the Time-domain Solver.

2.3.1 Prototype I-PIFA center

In this subsection, we present a dual-antenna design of the Slot-M antenna and PIFA for dual-band operation, which are LTE Band 13 (with center frequency F_c of 750 MHz) and LTE Band 7 (with center frequency F_c of 2.65 GHz). The reason for choosing the 750 MHz as the center frequency is that the PIFA in this prototype has a very narrow bandwidth and it can not cover the whole bandwidth; therefore we have shifted the center frequency to the left to cover the downlink bandwidth.

The chassis consists of a 0.1 mm top copper layer and a 1.55 mm bottom FR4 layer with a permittivity of 4.7 and a loss tangent of 0.015 [1].

Slot-M antenna

Figure 2.1 shows the dimensions of the proposed Slot-M antenna for mobile phone application. The two monopole slots are chosen for different frequency bands, the shorter slot used for the high band and the longer one (bent into the inverted-L shape to fit to the ground plane) is for the low band.

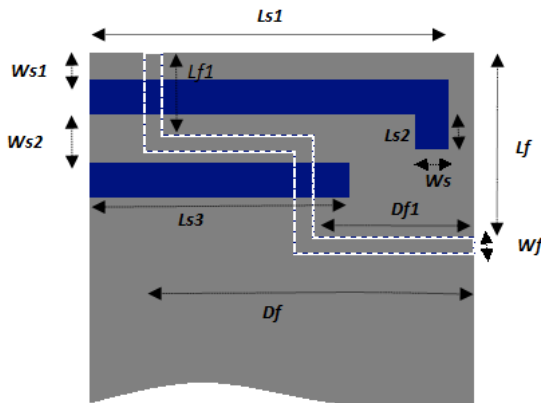


Figure 2.1: Geometry of Slot-M antenna: $Ls1=46.5mm$, $Ls2=1mm$, $Ls3=38mm$, $Ls1=46.5mm$, $Df=55.2mm$, $Df1=34.7mm$, $Lf=27.2mm$, $Lf1=9.7mm$

The lower band can be controlled by $Ls1+Ls2$ and the upper band by

Ls3. These slots have a width of 5 mm (*WS*), which determines the widening of the bandwidth for the lower and upper bands.

It has been conclusively shown in [2] that *WS1* has a considerable effect on the return loss for the lower and upper bands and a value of 4 mm is suggested. Thus to achieve good return loss behaviour *WS1* and *WS2* are chosen to be 4 mm and 7 mm, respectively.

To excite the two monopole slots, a 50- Ω microstrip feed-line is used to feed the two slots at the optimized locations along the slots (see Fig. 2.1) The width of tuning-stub (*Wf*) is chosen to be 2.8 mm. A parametric study of the *Df* value in [2] shows that *Df* has a large impact on the return loss. A proper selection of *Df* is thus essential to achieve good excitation for both monopole slots. For a larger value of *Df* better matching for the upper band has been obtained. Since our ground plane size is larger than the older candy-bar phones (100 x 40 mm²), *Df*, *Lf* and *Ws2* have been modified to achieve good matching for both bands.

We have replaced the straight strip line (*Lf*) in [2] with a meandered strip line as shown in Figure 2.1. The reason behind this change is that the current distribution for the low band as shown in Figure 2.2a has to flow from the closed end of the strip to the open end of the strip to have acceptable matching. Therefore according to the current distribution and parametric study in [2], *Df* and *Lf* have been divided into the two parts ($Df = Df1 + Df2$ and $Lf = Lf1 + Lf2$) and the exact values for *Lf1*, *Lf2*, *Df1* and *Df2* were optimized by trial-and-error.

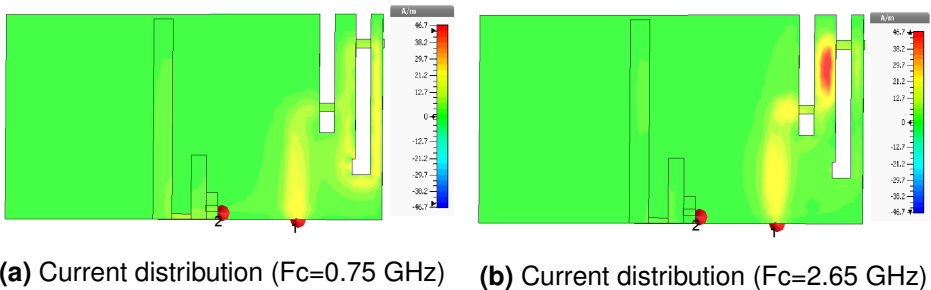


Figure 2.2: Current distributions of Slot-M antenna

PIFA

Figure 2.3 shows the PIFA structure with the corresponding geometries for Prototype I. The PIFA is integrated onto a hollow carrier (i.e., the shaded part), which is commonly used in mobile phones. The simulated carrier

has a thickness of 1 mm , a permittivity of 2.7 and a loss tangent of 0.007 [1].

A dual-band quarter-wavelength patch antenna generally has two branches for the lower and upper bands. As it can be seen from the structure in Figure 2.3 the shorter branch with the length of $L3$ controls the resonant frequency for the upper band, whereas on the other side the longer branch with the length of $L5$ determines the lower resonant frequency. For both bands, the widths ($W3$ and $W5$) control the antenna bandwidth.

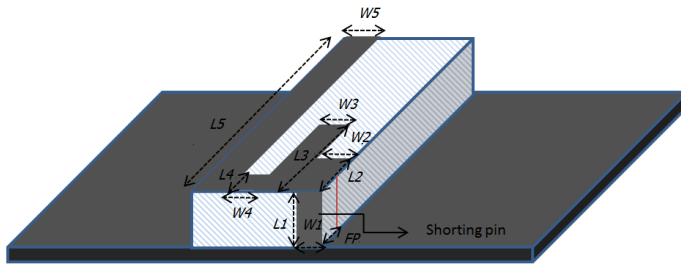


Figure 2.3: Geometry of the PIFA: $L1=7.4\text{mm}$, $L2=8.5\text{mm}$, $L3=20.6\text{mm}$, $L4=1.65\text{mm}$, $L5=64\text{mm}$, $W1=W2=3.78\text{mm}$, $W3=5.14\text{ mm}$, $W4=W5=6.37\text{mm}$

In the design of the PIFA, the input impedance is generally controlled or tuned by changing the width of the shunting pin and the gap between the feeding point and shunting pin. Based on the current distribution shown in Figure 2.4, the width of the shunting pin should be large enough to let the current flow into the longer branch. On the other hand, it should not be too large, since it will degrade the matching for the upper band. So we should consider this trade-off to achieve a proper value for both bands. Another essential parameter is the feeding point distance FP , where for small distances the lower band is well tuned and for large values the upper band has better performance, so the final value has been found by trial-and-error.

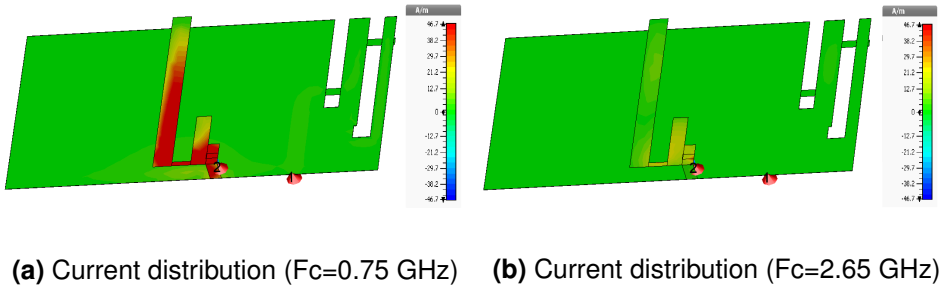


Figure 2.4: Current distributions of PIFA

The other parameters that should be considered for good matching are L_2 and L_4 . For small values of L_2 , the lower band works well but the upper band will be de-tuned. The reason behind this behaviour is that the small surface of the first strip line does not let the current flow properly through the high frequency branch. The value for L_2 has been chosen for both the low and high frequency bands by a parameter sweep. The value for L_4 should be small according to the current distribution. A small value will lead to the current flowing both into the lower and upper band branches. On the other hand, if the value is large, e.g., 3 mm, the main current will flow through the low frequency branch and the upper band will have poor performance. The optimum value for this length is chosen to be 1 mm.

S-parameters results

Generally for mobile phone antennas, the reflection coefficient threshold is defined to be -6 dB. Therefore the antenna bandwidth of antenna i is defined as the frequency range where the reflection coefficient S_{ii} is less than the threshold.

The scattering or S parameters for the first prototype in free space are shown in Figure 2.5 for Band 13 and Band 7. Figure 2.5a shows the results for Band 13 with the center frequency of 0.75 GHz. The Slot-M antenna is located on port one and the PIFA is located on port two. As it can be seen from the results, Slot-M is relatively wide-band as compared to the narrow-band PIFA. The results for the Band 7 are shown in Figure 2.5b. In this band the PIFA has a larger bandwidth as compared to the low band. The center frequency for this band is fixed at 2.65 GHz.

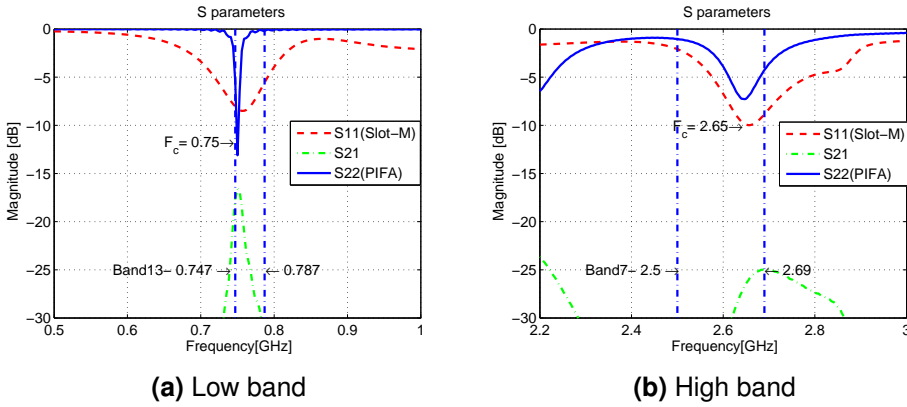


Figure 2.5: S parameters for Prototype I in free space

This prototype has high antenna isolation of above 15 dB, although this phenomenon contradicts the usual relationship between the inter-antenna distance and isolation. This result can be explained by Characteristic Mode Analysis [1], which shows that the total electric field of the first characteristic mode of the chassis has the maximum E-field value at the short edges and the minimum value at the center. Therefore the chassis is not efficiently excited by the PIFA and it is only utilized as the main radiator by the Slot-M antenna at the chassis edge.

2.3.2 Prototype II-PIFA rotated-center

In the second prototype, the PIFA is positioned at the center. But it is rotated by 90° with respect to the PIFA of Prototype I and it is positioned along the chassis long edge. The Slot-M antenna is located at the short edge of ground plane, as illustrated in Figure 2.6. Since the location of the PIFA was changed with respect to Prototype I, the new prototype needed additional tuning in order to fulfil the bandwidth requirements. For Prototype II and Prototype III, the center frequency was tuned to 767 MHz for Band 13.

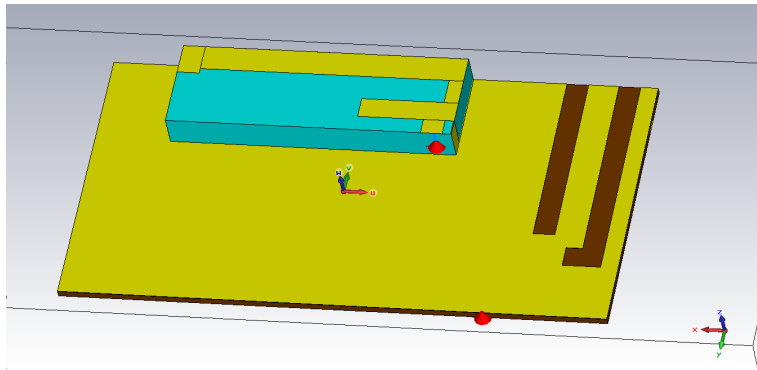


Figure 2.6: Structure of Prototype II

It can be observed from Figure 2.6 that the length of the longer branch for the PIFA is changed and the proper value for L_5 (see Fig. 2.3) is determined to be 67 mm . The Slot-M antenna has the same position and dimensions as the one in Prototype I.

The results obtained from the preliminary simulation of the antennas, S-parameters for Prototype II are shown in Figure 2.7. In the low band the PIFA and Slot-M antenna have a reflection coefficient of -12 dB and -13 dB , respectively, at the center frequency. Due to the antenna location along the chassis edge, the PIFA has a larger bandwidth at the center-rotated position as compared to the center position. The upper band is well matched for both antennas. As seen on Figure 2.7b, the PIFA and Slot-M antennas have a reflection coefficient of -15 dB and -16 dB , respectively, at the center frequency.

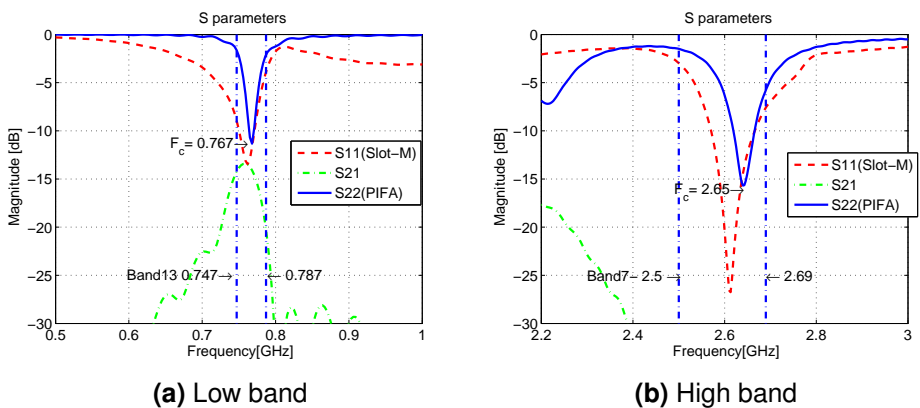


Figure 2.7: S parameters for Prototype II in free space

The maximum coupling between the antenna elements is -13 dB , which

is higher than for Prototype I. The higher coupling is due to the ground plane effect. The E-field distribution on the ground plane has its maximum value at the short edges and minimum value at the center. Therefore when the antenna is rotated at the center, the ground plane will be more excited by the PIFA then in the case of Prototype I and as a result the coupling between the antenna elements will become higher.

2.3.3 Prototype III-PIFA edge

The following subsection shows the last prototype investigated in this project. The PIFA is located at the short edge of the mobile chassis, while the Slot-M is located at the other short edge of the ground plane. The structure is shown in Figure 2.8.

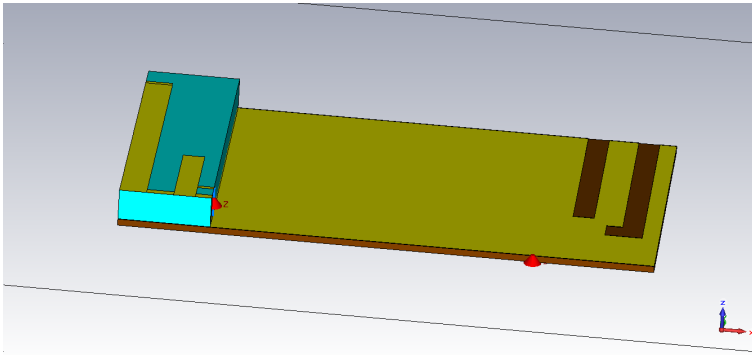


Figure 2.8: Structure of Prototype III

The results of the S parameters for Prototype III in free space are illustrated in Figure 2.9. Figure 2.9a indicates that both antenna elements are well matched and cover the entire Band 13. On the other hand, the coupling is the highest among all three prototypes. From our discussion in Section 2.3.2 on E-field distribution, we know that the maximum E-field value will be at the short edges of the chassis. Therefore, with the geometry of Prototype III, both antennas will excite the ground plane simultaneously and this will result in high bandwidth and high antenna element coupling.

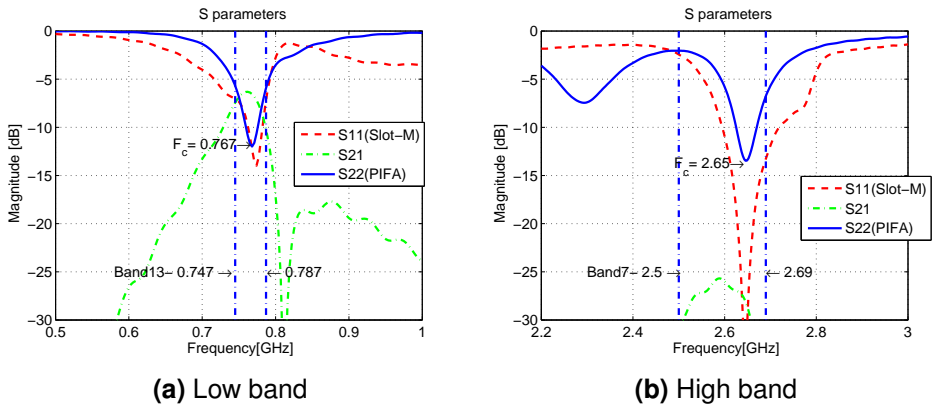


Figure 2.9: S parameters for Prototype III in free space

The results for the high band are shown in Figure 2.9b. Both PIFA and Slot-M antenna are tuned for the center frequency of Band 7 ($F_c = 2.65$ GHz). In this frequency band the antenna coupling is very low (~ -26 dB).

2.4 Measures of performance

2.4.1 Efficiency

The total radiation efficiency is decomposed into reflection losses and material losses [7]. Reflection losses is due to impedance mismatch between the transmission line and the antenna. Material losses consist of conduction and dielectric losses. Total efficiency can be written as

$$e_{tot} = e_{ref}e_c e_d, \quad (2.1)$$

where

e_{tot} = Total efficiency

e_{ref} = Reflection efficiency

e_c = Conduction efficiency

e_d = Dielectric efficiency.

Generally e_c and e_d are difficult to compute separately and it is usually more convenient to consider them as a single term called radiation efficiency

$$e_{rad} = e_c e_d. \quad (2.2)$$

Therefore, a simplified equation for the total radiation efficiency can be written as

$$e_{tot} = e_{rad}e_{ref} = e_{rad}(1 - |S_{11}|^2 - |S_{21}|^2). \quad (2.3)$$

The simulated results on radiation efficiency and total efficiency at the center frequency for both antennas of the three prototypes are shown in Table 2.1 and Table 2.2, respectively, for the free space scenario.

Case	P1 (%)	P2 (%)	P3 (%)
Radiation efficiency of PIFA	76.62	66.25	67.82
Radiation efficiency of Slot-M	76.66	86.75	90.82

Table 2.1: Radiation efficiency (free space)

Case	P1 (%)	P2 (%)	P3 (%)
PIFA	63.52	62.9	46.77
Slot-M	72.43	68.5	63.11

Table 2.2: Total efficiency (free space)

As it can be seen from Table 2.1 and Table 2.2, the radiation efficiency of Prototype III is the highest among the other prototypes for the Slot-M antenna element. On the other hand for the PIFA, Prototype I has the maximum radiation efficiency. Although Prototype III has the highest radiation efficiency for the Slot-M antenna element, the total radiation efficiency is the lowest for this prototype. This can be explained by the fact the Prototype III has the lowest isolation among the three prototypes, which leads to high coupling loss and low total efficiency.

2.4.2 Correlation

The study of correlation is essential for multiple antennas which are closely spaced due to the mobile chassis size limitation. To enable diversity for a MIMO system, the signals received at the antennas should be as independent of one another as possible. In other words they should have low correlation. In real world systems, the received signals are never completely independent of one another. Therefore, the concept of the correlation becomes increasingly important when we discuss realistic MIMO

systems. Usually, there are two methods to calculate envelope correlation in a uniform propagation environment. One is based on the far-field patterns and another one is based on the S parameters.

The envelope correlation based on far-field patterns is defined as [9]

$$\rho_e = \frac{(\int (XPR E_{\theta X}(\Omega) E_{\theta Y}^*(\Omega)) P_{\theta}(\Omega) + E_{\phi X}(\Omega) E_{\phi Y}^*(\Omega)) P_{\phi}(\Omega) d\Omega)^2}{\int (XPR G_{\theta X} P_{\theta}(\Omega) + G_{\phi X} P_{\phi}(\Omega)) d\Omega \cdot \int (XPR G_{\theta Y} P_{\theta}(\Omega) + G_{\phi Y} P_{\phi}(\Omega)) d\Omega}, \quad (2.4)$$

where $\Omega = (\theta, \phi)$, $d\omega = \sin(\theta) d\phi d\theta$, $G_{\theta} = E_{\theta}(\Omega) E_{\theta}^*(\Omega)$, $E_{\theta X}(\Omega)$ and $E_{\theta Y}(\Omega)$ are the θ polarized complex radiation patterns of antenna X and antenna Y (similar definitions apply to the ϕ -polarized parameters). $P_{\theta}(\Omega)$ and $P_{\phi}(\Omega)$ represent incident power spectrum for both polarization and XPR is the cross polar discrimination [9].

Computation of the correlation metric described above requires radiation pattern calculations and involves integral calculations, therefore it is a very time consuming method. The other method which is based on S-parameters is much faster than the far-field method and has been derived in [10].

$$\rho_e = \frac{|S_{11}^* S_{12} + S_{21}^* S_{22}|^2}{(1 - (|S_{11}|^2 + |S_{21}|^2))(1 - (|S_{22}|^2 + |S_{12}|^2))}. \quad (2.5)$$

In this project the correlation has been calculated by the far-field pattern method, since it is more accurate. This is because the S-parameter approach assumes lossless antennas, which is hardly the case for the antennas studied in this thesis. The correlation results for the three different cases are shown in Table 2.3.

Case	P1	P2	P3
Envelope correlation	0.0289	0.0408	0.38

Table 2.3: Correlation coefficient (free space)

The best place to locate the antenna in order to have low correlation coefficient is at the center according to the correlation results in Table 2.3. This can be explained by the way the ground plane is being excited. It has been mentioned in Section 2.3.3 that the maximum value of the E-field is at the short edges of the chassis. Therefore, if the PIFA is placed at the center it will not be exciting the chassis simultaneously along with the Slot-M and this would result in low correlation. Prototype III has the highest correlation coefficient, because both antennas are located at the short edge

and are exciting the ground plane simultaneously. Finally, Prototype II has a correlation coefficient between Prototype I and Prototype III and that can be attributed to the antenna locations on the mobile chassis.

2.4.3 Radiation Pattern

An antenna radiation pattern or antenna pattern is defined as a "mathematical function or a graphical representation of the radiation properties of the antenna as a function of space coordinates" [7]. We have used the 3D patterns, which are mapped to 2D figures.

Prototype I radiation pattern

It can be concluded from Figure 2.10 that both antennas have almost omnidirectional patterns.

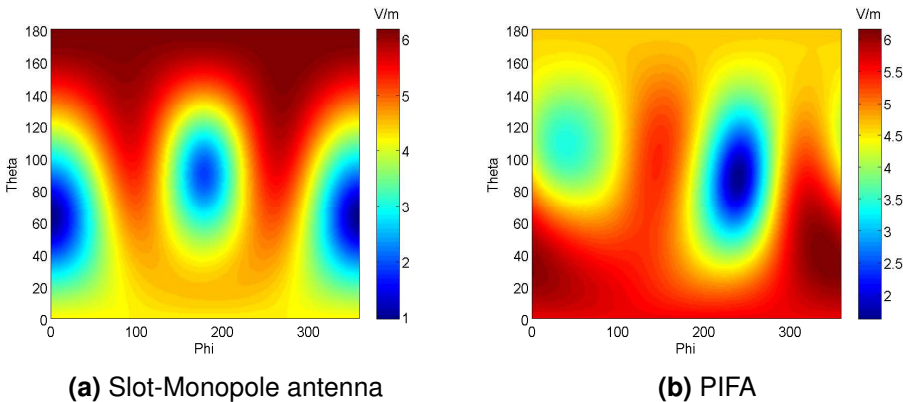


Figure 2.10: Radiation pattern of Prototype I at 750 MHz

Prototype II radiation pattern

In Figure 2.11 we see that the Slot-M antenna for Prototype II has a similar radiation pattern as Prototype I with a slightly lower maximum E-field magnitude. On the other hand, the PIFA has a different radiation pattern than that in Prototype I due to the location of the antenna.

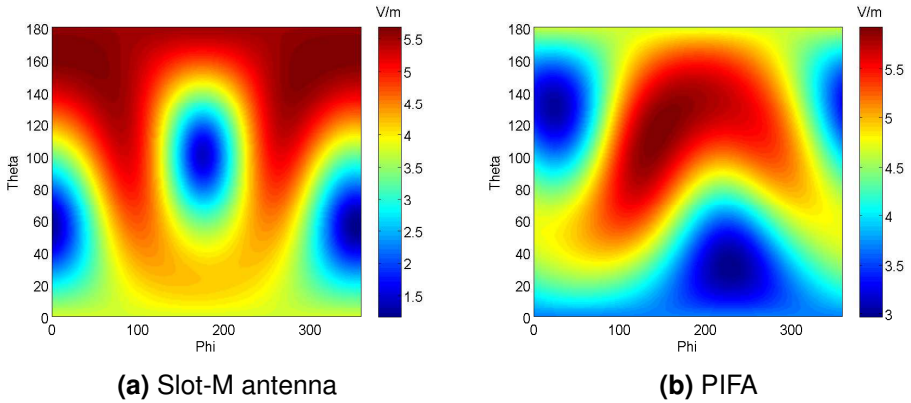


Figure 2.11: Radiation pattern of Prototype II at 767 MHz

Prototype III radiation pattern

For the last prototype, we can expect the same pattern for the Slot-M antenna, because of the same location of the antenna. Meanwhile, the radiation pattern of the PIFA is different pattern compared to the other prototypes as shown in Figure 2.12.

It can be concluded from the radiation pattern results that Prototype I has the highest maximum E-field magnitudes as a result of the high total efficiencies for both antennas.

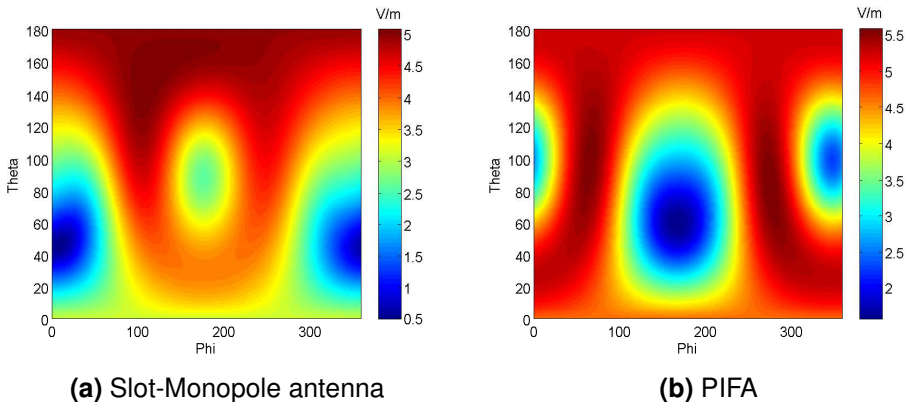


Figure 2.12: Radiation pattern of Prototype III at 767 MHz

User Effect Study

3.1 User effect overview

User interaction is very important in wireless and mobile systems. In fact handheld phones experience significantly higher losses in the link budget as compared to the similar car mounted phones [11]. These losses are mainly attributed to body-loss, which is the ratio of the received power by the mobile device with the user present to the power received in the absence of the user.

There are four factors that contribute to the body-loss [11]

- Absorption, usually presented as Specific Absorption Rate (SAR)
- Antenna detuning
- Change of radiation direction
- Change of polarization state

Absorption is dependent on the person who holds the mobile device and is the main cause of the body-loss. Variations in the absorption caused by users can be classified according to: hand position, head to phone distance, phone tilt angle, hand and head shape, age, gender, etc. [11]. Since our focus is on antenna parameters such as radiation efficiency and antenna mismatch loss, we will not focus on SAR results.

Having a realistic hand model is essential for evaluating antenna performance. In the beginning of this project, CST hand models were chosen for our study. There are two types of CST models: the fixed grip model suitable for the "bar" mobile-phone size ($100 \times 40 \text{ mm}^2$), and the flexible grip model, which can be adjusted for different mobile-phone sizes.

Even though these models are used by CTIA (Cellular Telecommunications Industry Association) to define specific hand grips, they do not cover the multiple grip positions that we planned to test in this study. Therefore, we came with an alternative solution that is a custom designed hand model done in the Makehuman 3D-software.

Three different scenarios are chosen to evaluate the designed antenna prototypes: data mode (one hand), game mode (two hands) and talk position (one hand). The grip positions used in this study are based on [4]. The investigation on user effect is only performed for LTE Band 13, since the user induced performance degradation is much more significant for lower frequencies.

3.2 Hand phantoms

3.2.1 Models

In this section we address the difficulties in using hand models for different hand postures and propose a solution for it. CST Microwave Studio provides two types of hand models. The first type is the inhomogeneous model that can only be used for "bar" mobile-phone sizes (usually chassis of $100 \times 40 \text{ mm}^2$). The second type is the homogeneous model with flexible grip, which do not provide complete freedom to change the grip position in different directions. Instead, this model only allows for changes in the hand grip opening, so that different mobile phone sizes can be accommodated. The advantage of this model is that the mobile device can be easily located on the spacer, which is included in the model.

Both of these models do not satisfy our requirements, which are appropriate models for three different user scenarios.

3.2.2 Makehuman models

Makehuman is a 3D-modeling software, which has an easy user-interface and provides total freedom to change the hand grip to any realistic position. It has an option to change the sex, body mass and body shape. Once the model has been modified, it can be exported as an object file (.obj). Moreover there is an option for saving customized poses, so that it can be applied to another future model. The model can be easily imported to CST Microwave Studio and the material properties of the hand can then be defined. The hand material is chosen according to the CST homogeneous hand model.

Figure 3.1 shows a screen shot from the Makehuman software, which shows the hand model, as well as the interface and the options.



Figure 3.1: Makehuman software

3.3 One-hand scenarios

To cover more scenarios for the one hand case, two grip positions were chosen: data mode and talk mode.

3.3.1 Talk Mode

The grip style for the talk mode is based on [4]. The investigation in [4] shows that most of the users hold the phone according to Figure 3.2. While talking, the index finger is located in the back region of mobile phone. The thumb usually holds the phone from the side and is located in the middle. On the other hand, the middle finger is located at the same level as the thumb on the other side of the phone. The little finger may not be in contact with the phone and is located at the right-end of the phone. Finally the ring finger is located above the little finger. It can be concluded that the hand holds the phone with only the distal phalanges.

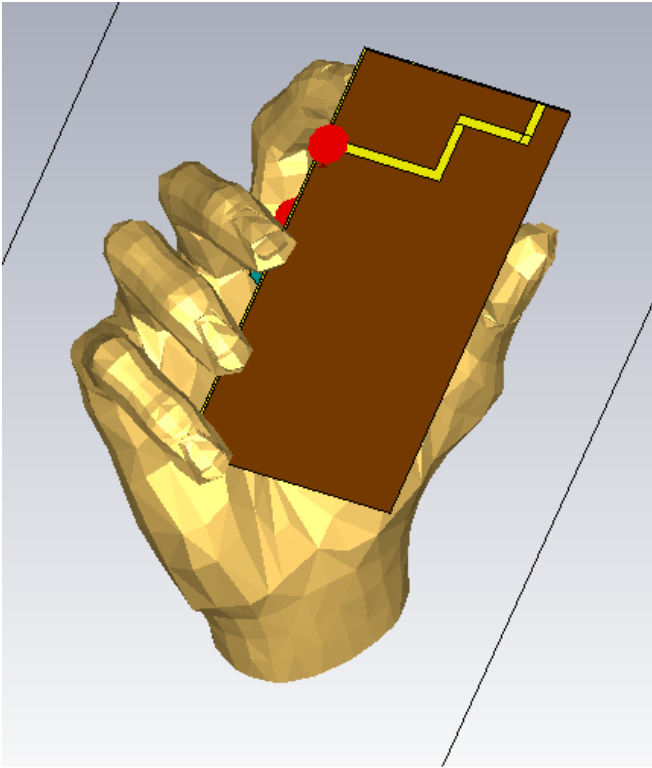


Figure 3.2: One hand talk mode scenario

The results of the antennas simulation for the talk mode scenario are shown in Figure 3.3, Figure 3.4 and Figure 3.5.

Prototype I

The results of the antennas simulation for the talk mode scenario are shown in Figure 3.3. It can be seen that the reflection coefficient of the PIFA is shifted to below the center frequency. Due to the effect of the palm on the PIFA, it is detuned at the center frequency. On the other hand, the Slot-M antenna is not as much affected by the hand and is still well-matched at the center frequency with $S_{11} = -13$ dB.

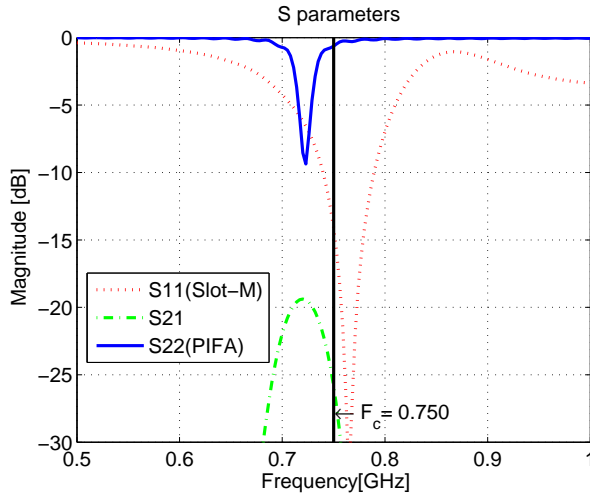


Figure 3.3: S parameters of Prototype I in talk mode

Prototype II

Figure 3.4 presents the simulation results for the second prototype. In this prototype, the PIFA has a better performance as compared to Prototype I. However, it is still detuned at the center frequency ($S_{11} = -4.5$ dB). The Slot-M antenna is still well-matched at the center frequency. The mutual coupling is higher than the previous case and is equal to -15 dB.

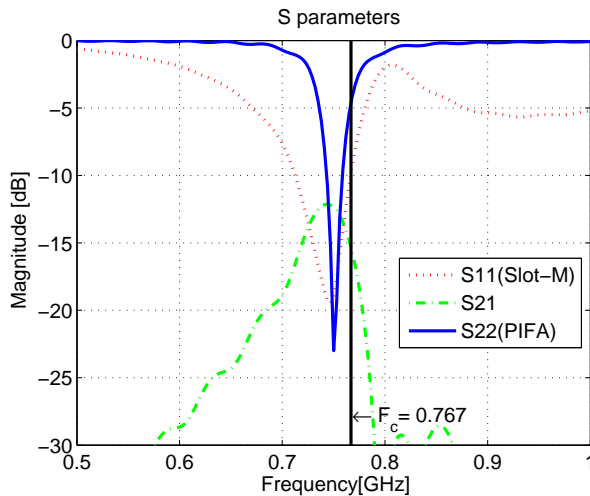


Figure 3.4: S parameters of Prototype II in talk mode

Prototype III

Figure 3.5 presents the S-parameter results of Prototype III. It is observed that the Slot-M antenna and PIFA are working at the center frequency with the return losses of -16.45 dB and -7.5 dB, respectively. However, this prototype has the highest coupling among the other prototypes with a value of -9.26 dB.

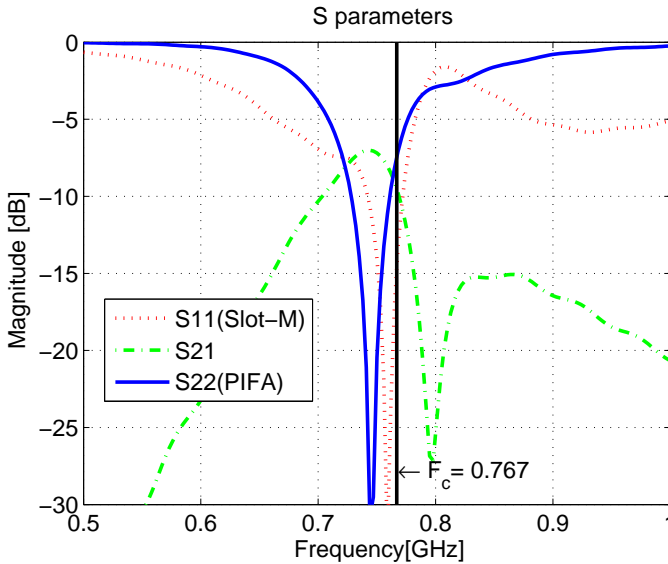


Figure 3.5: S parameters of Prototype III in talk mode

3.3.2 Data Mode

For the data mode, the grip position which is shown in Figure 3.6 is slightly different from the talk mode. In this case, the thumb is located on the top of the screen region. The pinky is at the bottom of the phone and is holding the phone. The middle and ring fingers are above the little finger and are located close to the center of the chassis width. The index finger is a bit further away from the middle finger.

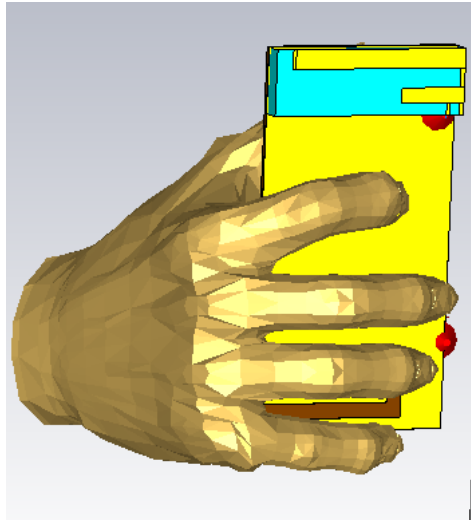


Figure 3.6: One hand data mode scenario

Prototype I

It can be seen from Figure 3.7 that the PIFA is severely detuned. This is due to the fact that the antenna is entirely covered by the hand in this user scenario. Nevertheless, the Slot-M antenna is barely affected by the hand and is well matched at the center frequency ($S_{11} = -10$ dB). It is noteworthy that the coupling is below -25 dB in this case.

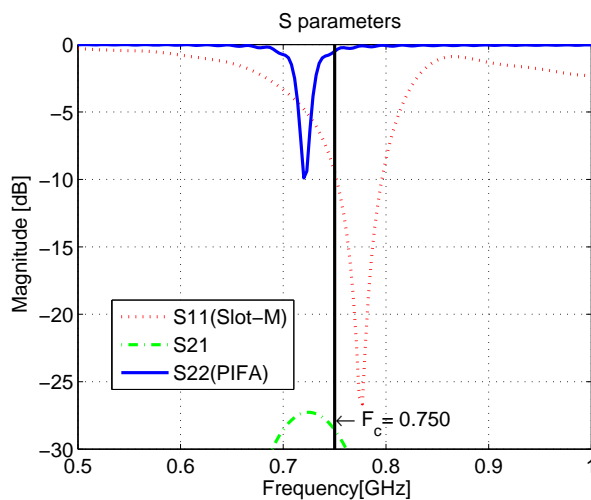


Figure 3.7: S parameters of Prototype I in data mode

Prototype II

The performance of Prototype II in the data mode scenario is illustrated in Figure 3.8. Both antennas are detuned at the center frequency, due to the strong influence of the hand grip.

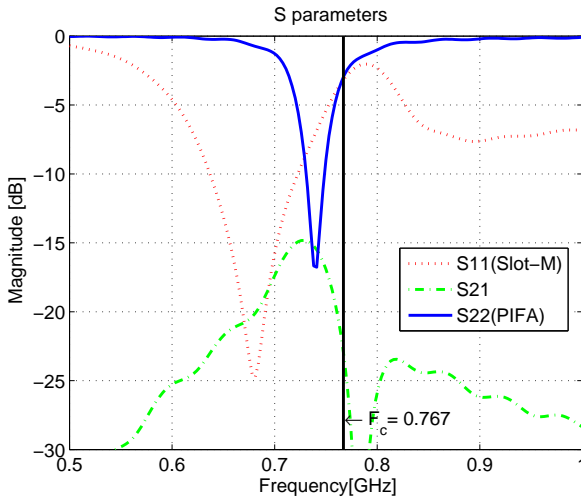


Figure 3.8: S parameters of Prototype II in data mode

Prototype III

Figure 3.9 presents the S-parameter results for the last prototype. This prototype shows the lowest isolation of 15 dB. In addition the Slot-M antenna is detuned at the center frequency due to the hand affect. On the other hand, the PIFA is not affected by the hand and is still well-matched at the center frequency as it can be seen from the S parameters.

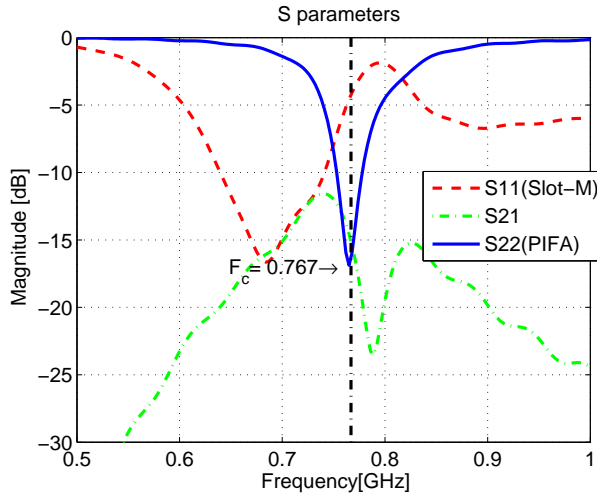


Figure 3.9: S parameters of Prototype III in data mode

3.4 Two-hand scenario

Another grip style is when the right and left hands are involved. In this scenario the phone is rotated by 90° and the hands are holding the phone at both short edges. The grip position is designed according to the experiment done in [12]. As it can be seen from Figure 3.10, the index and middle fingers are holding the phone from the back side, while the ring finger and pinky are holding the phone from the bottom. This scenario can also be referred to as game mode.

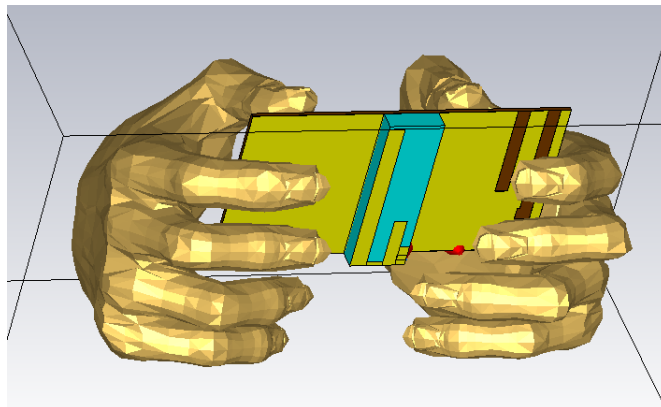


Figure 3.10: Two hand (or game mode) scenario

The results obtained from CST Microwave Studio simulations for the

three different cases are presented in Figure 3.11, Figure 3.12 and Figure 3.13. In all the cases, the PIFA is affected by the hands and is not resonating at the center frequency. Prototype I has the lowest performance among the other prototypes. On the other hand, the Slot-M antenna is still working in all the cases with similar matching characteristics for all three prototypes ($S_{11} \sim -11$ dB). Moreover, the first and third prototypes have the lowest and highest mutual coupling values, respectively.

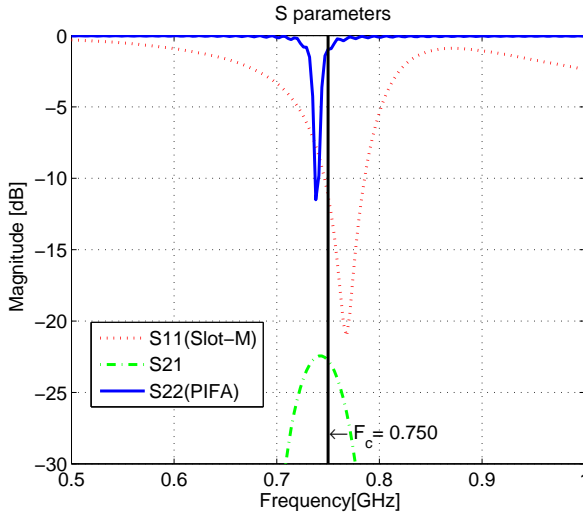


Figure 3.11: S parameters of Prototype I in game mode

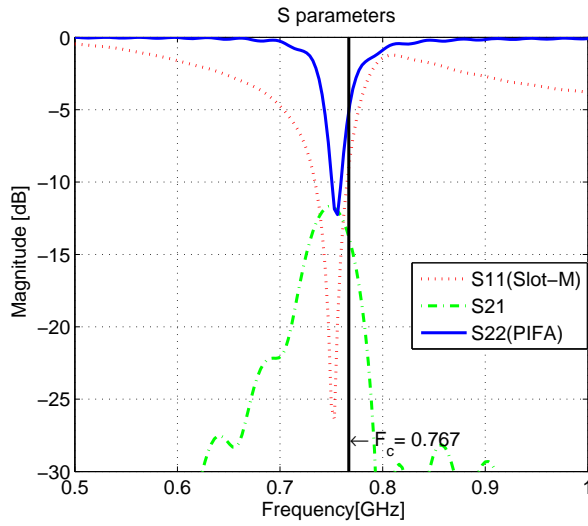


Figure 3.12: S parameters of Prototype II in game mode

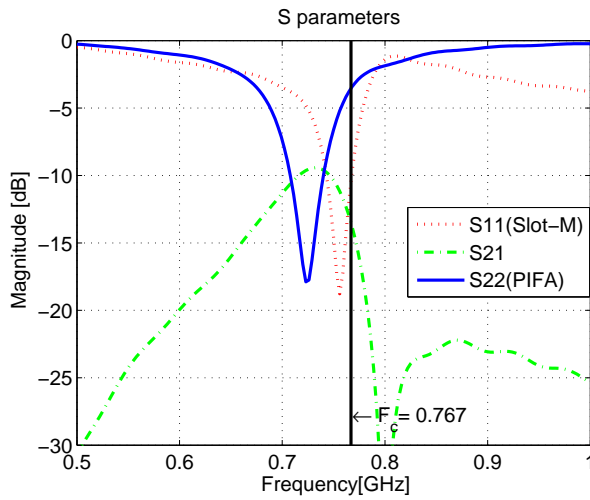


Figure 3.13: S parameters of Prototype III in game mode

Adaptive Impedance Matching

4.1 Introduction

In this project we propose adaptive impedance matching as a method to improve antenna performance. Impedance matching can be used to optimize different criteria e.g. to maximize transferred power, to minimize reflection coefficient, maximize capacity, etc. Therefore based on our project goal, we have focused on capacity improvement and applied the proposed method to optimize capacity. The algorithm used in this analysis assumes limited number of impedance states, as can be seen in Figure 4.1.

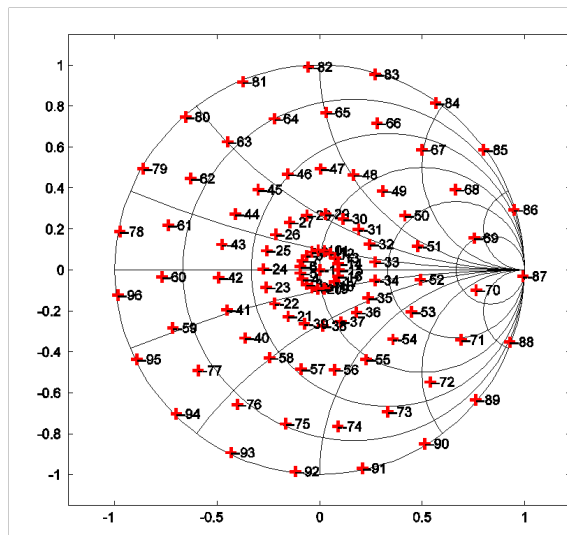


Figure 4.1: Considered states in Smith chart

In total there are 96 states, which start from 50Ω (Initial state) and end with the 96th state located on the most outer part on the Smith chart. For each state, the antenna radiation pattern is updated and from the radiation

pattern other performance metrics such as efficiency and correlation are calculated.

4.2 Principle of Operation

The antennas with the adaptive impedance matching (AM) networks are shown in Figure 4.2.

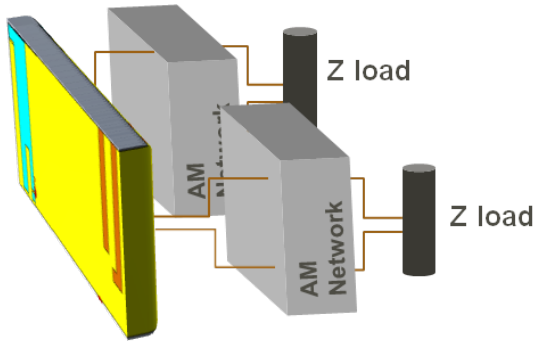


Figure 4.2: Antennas and adaptive impedance matching networks

The embedded element pattern for a single antenna element in a multi-port antenna is the radiation pattern, when the selected antenna element is excited and all the other antenna elements are terminated with the standard 50Ω impedance. For the 2x2 MIMO antenna system in this project the evaluation algorithm is as follows [13].

1. Excite element 1 and terminate element 2. Compute $E1$ (embedded element pattern for element 1)
2. Excite element 2 and terminate element 1. Compute $E2$ (embedded element pattern for element 2)

When the impedance matching networks are added, the embedded element patterns for the antennas with the networks can be calculated from the case without the networks, given the S parameters of the networks [13]. This calculation is updated for every matching state and the corresponding antenna parameters such as efficiency and correlation are calculated from radiation patterns with matching networks. The efficiency is divided into two components: radiation efficiency and total efficiency. The radiation efficiency is the ratio of the antenna gain to the antenna directivity. The total efficiency is calculated from the S parameters and the radiation efficiencies.

As mentioned in Section 3.4.2., correlation is computed from surface integrations of the far-field patterns.

4.3 Numerical study

4.3.1 Capacity

Considering a $M_r \times M_t$ MIMO channel \mathbf{H} , the channel capacity with no channel information at the transmitter (i.e. equal transmit power allocation) can be expressed as [15]

$$C = \log 2(\det(I_{M_r} + \frac{\rho}{M_t} \mathbf{H}\mathbf{H}^H)), \quad (4.1)$$

where I_{M_r} is the identity matrix of size $M_r \times M_r$, ρ is the signal-to-noise ratio and M_t (M_r) is the number of transmit (receive) antennas which in this project is two. The propagation environment here is assumed to be independent and identically distributed (i.i.d.) Rayleigh fading channel H_w . The entries of H_w are zero-mean circularly symmetric complex Gaussian random variables. Correlation effects in the receive antennas are included in the channel according to the Kronecker model and follow the derivations in [16]

$$\mathbf{H} = \mathbf{R}^{1/2} \mathbf{H}_w, \quad (4.2)$$

where \mathbf{R} is the receive correlation matrix. It takes into consideration antenna total efficiency and correlation to

$$\mathbf{R} = \Lambda^{1/2} \bar{\mathbf{R}} \Lambda^{1/2}, \quad (4.3)$$

where $\bar{\mathbf{R}}$ is a normalized correlation matrix whose diagonal elements are one, and the off-diagonal elements $\bar{\mathbf{R}}(i,j)$ denote the complex correlation coefficient between the 3-D radiation patterns of the i th and j th antennas [16]. Λ is a diagonal matrix given by

$$\Lambda = \text{diag}[\eta_1, \eta_2] \quad (4.4)$$

where η_1 and η_2 are the total efficiencies of the first and second antenna, respectively.

In this project we have assumed an SNR of 20 dB for calculating MIMO capacity. For each state the capacity is calculated according to (4.1). Finally, the state providing maximum absolute capacity is chosen as the optimal matching state

Results

Since the correlation between antennas is mostly low (i.e., less than 0.5) in the considered user scenarios, the capacity results are mainly influenced by the total efficiencies of the antennas. Therefore, in the following discussions, the focus will be on the impact of efficiency results on the capacity results.

5.1 Prototype I

5.1.1 Talk mode

In Figure 5.1a, the capacity for the 50Ω state and the capacity for the optimal states (over both antennas) are shown for the talk mode scenario. Capacity is calculated over the entire LTE Band 13 (i.e., 40 MHz bandwidth) with the optimal and 50Ω matching states determined for the center frequency. Total antenna efficiency results are shown on Figure 5.1b. The blue curves represent total efficiency results for the Slot-M antenna (with adaptive matching (AM) and without), while the red curves show the corresponding efficiency results for the PIFA.

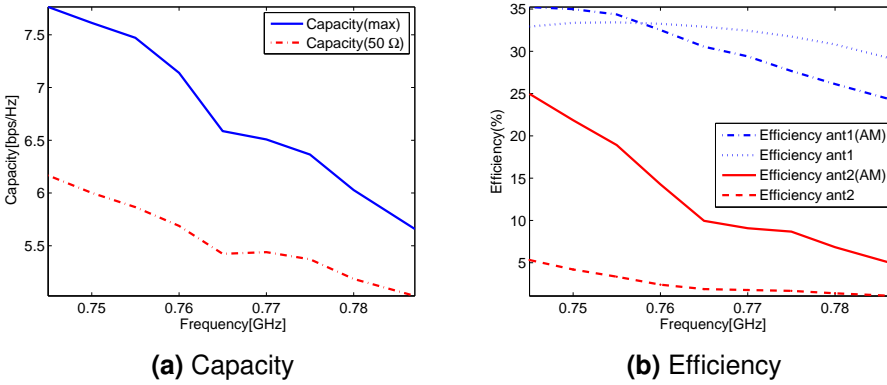


Figure 5.1: Capacity and efficiency for one hand talk mode (Prototype I)

It can be concluded from the capacity results that the absolute capacity decreases over the bandwidth for both $50\ \Omega$ and the optimal states. The gap between the $50\ \Omega$ capacity and the optimum capacity decreases as the frequency increases. This can be explained by the fact that capacity is dependent on the efficiency and the gap between the antenna efficiency for these two cases is decreasing as well. Moreover, the PIFA has a larger effect on the capacity, since it has the lower efficiency resulting from the user interaction. Furthermore, the S-parameter results in Figure 3.3 show that while the PIFA response is shifted to the left of the center frequency, the Slot-M antenna is well matched and not as severely influenced by the user. Detailed results for the talk mode scenario are shown in Appendix A.

5.1.2 Data mode

The results from the data mode simulations show the same trend as the talk mode scenario in terms of capacity and efficiency. Nevertheless, some minor differences can be observed. For instance, the Slot-M antenna in the data mode scenario has a higher efficiency as compared to the talk mode scenario. This is a result of the hand position in these two scenarios. In these two cases the hand covers both antennas in a different manner. In the data mode scenario, the antennas are facing the fingers, while in the talk mode scenario they are facing the palm which has a stronger effect on the antennas performance. The PIFA has a lower efficiency in the data mode than in the talk mode. The efficiency loss is due to the strong influence of the hand. Mean capacity gain over the bandwidth for the talk mode case is higher than the data mode, since the hand has a larger effect on

the talk mode and we can expect higher capacity gain for this scenario. The corresponding mean capacity values (over the 40 MHz band) for talk mode and data mode scenarios are 21.6 % and 19.2 %, respectively. Detailed results for the data mode scenario are shown in Appendix A.

5.1.3 Two hands

Figure 5.2 illustrates the capacity and efficiency of Prototype I (PIFA at the center) for the 50 Ω and optimal states.

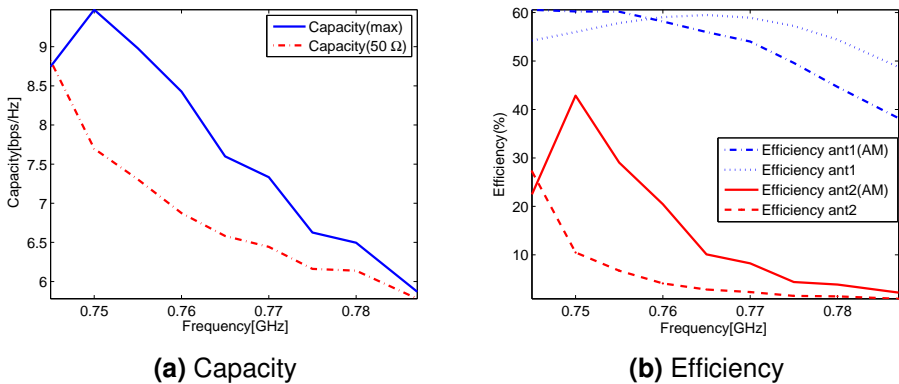


Figure 5.2: Capacity and efficiency for two hands (Prototype I)

From the results, it can be seen that at the start frequency (0.746 GHz), the absolute capacity for the initial state (50 Ω) and optimal state is similar. Nevertheless, the gap between these two matching states increases until its maximum which occurs at the center frequency of operation.

This tendency can be explained by the S-parameter and efficiency results. From the S parameters, it can be concluded that the PIFA has a better matching condition ($S_{11} = -5$ dB) at the start frequency, while for the rest of the band this condition deteriorates. Moreover, the efficiency of the PIFA at the start frequency is higher for the 50 Ω state compared to the optimal state. The highest capacity gain occurs at the center frequency, due to the fact that the adaptive impedance matching network is optimized for the center frequency. The mean capacity gain (over the 40 MHz band) for the two-hand scenario is 12.4%. Detailed results are given in Appendix A.

In general, the absolute capacity for Prototype I is considerably higher than for the rest of the prototypes, due to low correlation and high isolation.

5.2 Prototype II

Figure 5.3 shows the results obtained from the capacity and efficiency calculation for the second prototype (PIFA rotated at center) over the 40 MHz band in the talk mode scenario. As it can be seen from the capacity results in Figure 5.3a, the absolute capacity for the 50 Ω state has a higher value at frequencies below 0.762 GHz as compared to the optimal state capacity.

This can be explained by the S-parameter and efficiency results. The S parameters show that the PIFA has a better performance in frequencies below 0.762 GHz. Therefore, we expect to have a low capacity gain for frequencies below 0.762 GHz. These observations are confirmed by the efficiency results in Figure 5.3b, where the PIFA efficiency at the 50 Ω state is higher than that at the optimal state.

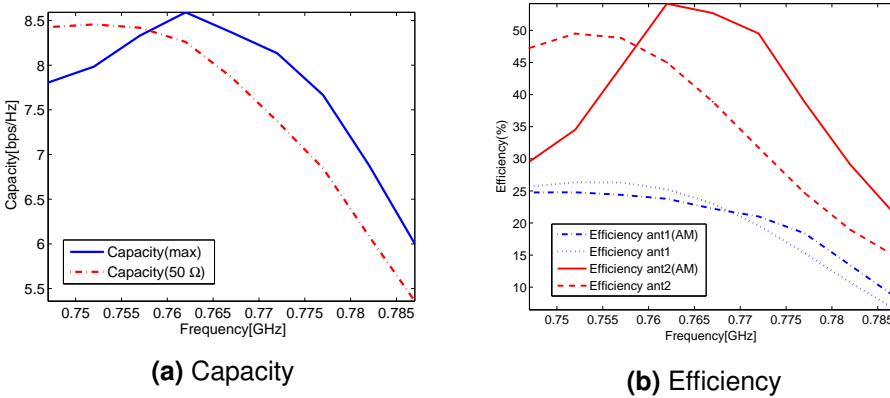


Figure 5.3: Capacity and efficiency for one hand talk mode (Prototype II)

The absolute capacity and capacity gain corresponding to the data mode and game mode (two hands) scenarios have a common tendency over the bandwidth with slightly different values. Differences in the hand grips in the data mode and game mode cause different values for the efficiency and capacity. In the data mode, the hand covers both antennas which degrades the antennas performance dramatically. As a consequence the mean capacity gain for the data mode has the highest value among all the user scenarios (18.1%). For the talk mode and game mode, the antennas are less affected by the hands. The mean capacity gain of the talk mode is similar to that of the data mode with a value of 4.8%. The game mode has the lowest mean capacity gain among all the scenarios (2%). Additional results for the data mode and game mode can be found in Appendix A.

5.3 Prototype III

5.3.1 One hand data mode

The results for the data mode for Prototype III are shown in Figure 5.4. It can be concluded from Figure 5.4a that the capacity gap between the 50 Ω states and the optimal state is highest in the proximity of the center frequency of operation. This result is expected since the matching networks are optimized for the center frequency.

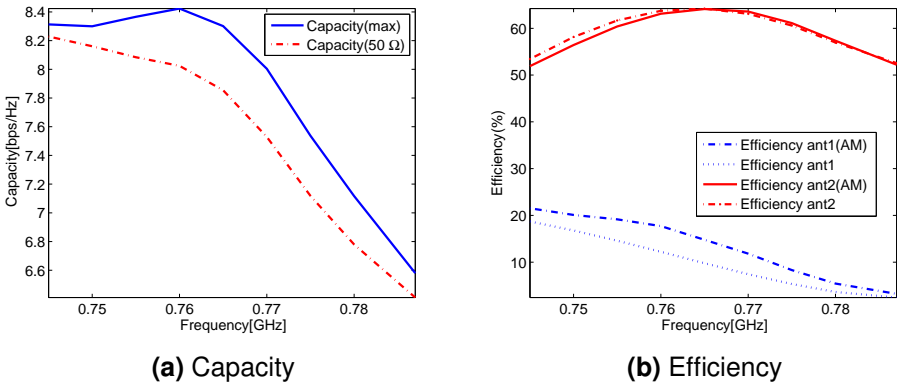


Figure 5.4: Capacity and efficiency for one hand data mode (Prototype III)

The efficiencies of both antennas are shown in Figure 5.4b. In this scenario, the hand grip has a stronger effect on the Slot-M antenna performance as compared to the PIFA. Therefore, the efficiency of the PIFA is higher than the Slot-M antenna. The highest capacity gain is obtained at the center frequency (6%), while the mean capacity over the bandwidth is improved by 4%.

5.3.2 One hand talk mode

In Figure 5.5, the results of the capacity and antenna efficiency in the talk mode are illustrated.

From Figure 5.5b it can be seen that the PIFA has a higher efficiency than the Slot-M antenna, since the hand grip has a larger effect on the Slot-M antenna. Nevertheless, both antennas are still well-matched at the center frequency.

For frequencies below 0.757 GHz, the capacity for the initial state has higher values than for the optimal states. This indicates that both antennas

have a good performance in this region. For frequencies above 0.757 GHz, the performance of the Slot-M antenna and PIFA starts to degrade and the capacity gap between the optimum state and 50 Ω state increases. The mean capacity for the PIFA at the edge (Prototype III) is 4.85 %. It is noteworthy that in this scenario the envelope correlation coefficient is about 0.4 over the bandwidth due to low isolation. As a consequence, the absolute capacity becomes low in the talk mode. The correlation results are shown in the Appendix A.

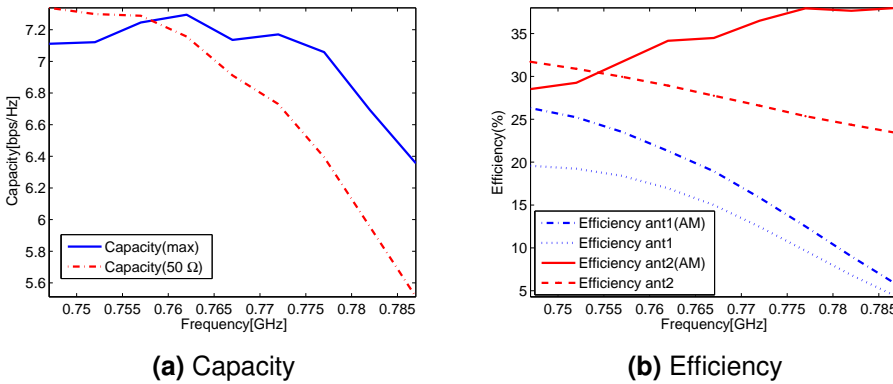


Figure 5.5: Capacity and efficiency for one hand talk mode (Prototype III)

5.3.3 Two hands

The results for the two-hand scenario (game mode) are illustrated in Figure 5.6. As shown in Figure 5.6b, the PIFA in the 50 Ω state has a lower efficiency than the Slot-M antenna. Whereas for the optimal state the PIFA has a higher efficiency than the Slot-M antenna. This shows that the impedance matching network improved the PIFA efficiency more than the Slot-M efficiency.

On the other hand, the S-parameter results show higher return loss values as compared to the other scenarios, which leads to a high capacity gain with the mean value of 8% over the bandwidth.

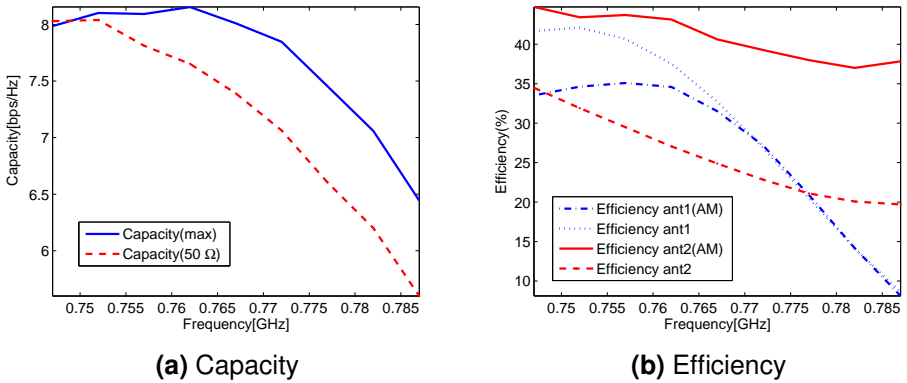


Figure 5.6: Capacity and efficiency for two hands (Prototype III)

5.4 Prototypes Comparison

5.4.1 Over the bandwidth-Two hands

In Figure 5.7 the efficiency results over the bandwidth for the three prototypes are shown. As seen from the results, Prototype I has the highest total efficiency for the Slot-M antenna. The third prototype has the lowest efficiency for this antenna and Prototype II has a moderate performance. In the case of the PIFA, Prototype I and Prototype II have the lowest and highest total efficiencies, respectively.

At the center frequency, Prototype I has the highest improvement in capacity among all three prototypes (23%). In particular, we can expect high capacity gain for the first prototype because it is severely affected by the hands. Prototype III has the lowest absolute capacity for the optimal matching states, due to the highest correlation in this prototype. Finally, the capacity gain of Prototype II is not as that of high as the other prototypes since this prototype is less affected by the hand grips.

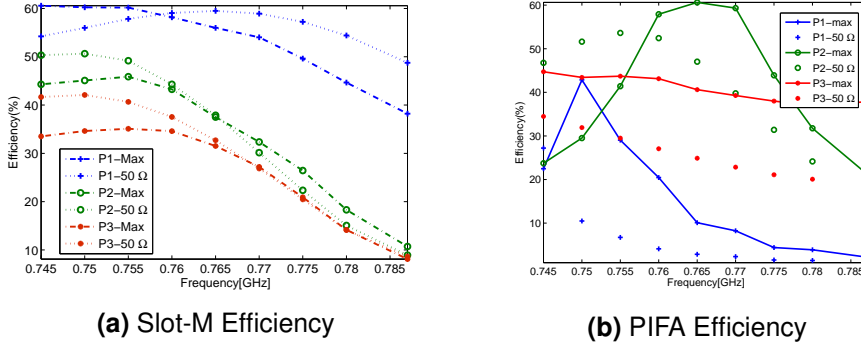


Figure 5.7: Efficiency for two hands (game mode)

It can be seen on Figure 5.8a that the second prototype has the highest average absolute capacity (for optimal states determined for the center frequency) around the center frequency as compared to the first and third prototypes. Due to the small influence of the hand grips in this prototype, both antennas have good performance in terms of efficiency and matching. Prototype I has a slightly lower average capacity around the center frequency as compared to Prototype II. Moreover, Prototype III has the lowest average capacity around the center frequency, due to the low efficiencies of the antennas and high correlation.

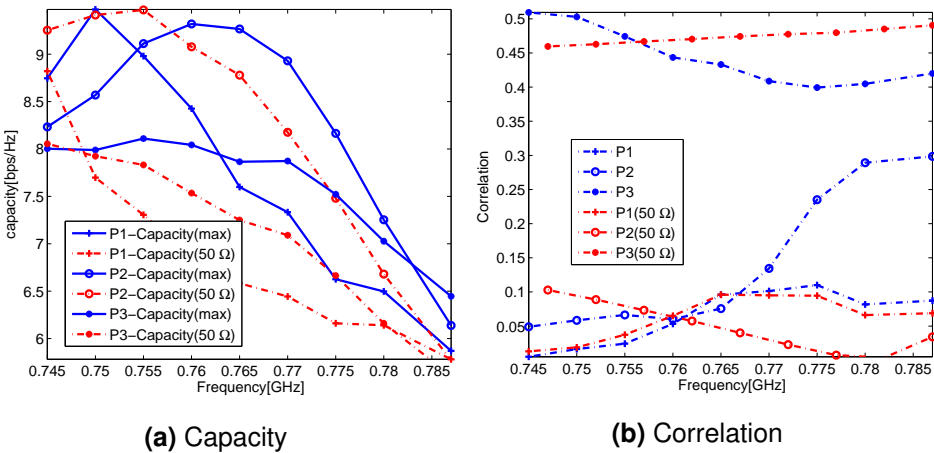


Figure 5.8: Correlation and capacity comparison

5.4.2 Results at the center frequency

The results of the antenna performance metrics (capacity, correlation and efficiency) are shown in Table 5.1 and Table 5.2 for the center frequency. The capacities and envelope correlation coefficients are shown for the 50 Ω state and the optimal states. The capacity gains are presented as percentage values for all prototypes in free space (FS), data mode (DM), talk mode (TM) and two-hand (TH) scenarios.

Metrics/Case		Capacity(50 Ω -Max,bps/Hz)		Capacity Gain(%)	Correlation coeff.(50 Ω -Max)	
P I	FS	10.1	10.5	2.1	0.02	0.01
	TM	6	7.7	27	0.25	0.29
	DM	6.2	8	26.5	0.15	0.142
	TH	7.7	9.5	23	0.019	0.016
P II	FS	10.1	10.3	2	0.07	0.04
	TM	7.6	8.4	7	0.25	0.13
	DM	5.9	7.5	23	0.03	0.01
	TH	8.7	9.2	5.7	0.22	0.1
P III	FS	9.2	9.4	2	0.37	0.17
	TM	6.8	7.1	4.5	0.22	0.4
	DM	7.87	8.3	5.7	0.04	0.038
	TH	7.4	8	8	0.47	0.42

Table 5.1: Capacity and correlation at center frequency

Metrics/Case		Efficiency(Slot-M)(50 Ω ,Max)(%)		Efficiency(PIFA)(50 Ω ,Max)(%)	
P I	FS	63.5	72.9	72.3	75
	TM	33.36	35	4.2	21.8
	DM	47.3	52	2.9	16
	TH	56	60	10.5	42.9
P II	FS	62.9	65.5	68.56	75
	TM	25.4	23.7	45	54.1
	DM	10.56	15.72	24.5	37.1
	TH	44.3	43.2	52.4	58
P III	FS	48.23	46.4	63.3	60
	TM	17	21.3	28.9	34
	DM	9.7	15	64	64
	TH	37.5	34.6	27	43

Table 5.2: Total efficiency of the three prototypes at center frequency

From the results at the center frequency, it can be concluded that Prototype I has the highest absolute capacity for the optimal states in most of the user scenarios. The capacity gain for this prototype is over 20% in all the hand scenarios. The high absolute capacity comes from the high efficiency of the antennas in this prototype, especially the Slot-M antenna.

On the other hand, the PIFA has a low performance and is detuned at the center frequency; therefore we can expect high capacity gains from adaptive matching. The results in Table 5.1 confirm this conjecture.

For Prototype II, the absolute capacity is slightly lower as compared to that of the prototype with PIFA at the center (Prototype I). The capacity loss comes from the efficiency difference. In Prototype II, the capacity gain is lower compared to the first prototype, since it is less affected by the hands and the antennas have better matching at the center frequency. The correlation for Prototype II and Prototype I are consistently low for all the user scenarios.

The last prototype has the lowest absolute capacity and capacity gain in most of the cases. This can be explained by the low efficiencies of the antennas which lead low absolute capacities. On the other hand, Prototype III has the largest bandwidth among all the prototypes, which makes it more robust to user effects. Nevertheless, the correlation in this prototype is relatively higher than that in the other prototypes due to the ground plane excitation phenomenon described earlier in the report.

Conclusion

In this thesis project, we have designed three different dual-antenna prototypes for the LTE Band 7 and Band 13. These prototypes have been evaluated in four user scenarios. Furthermore, adaptive impedance matching is proposed in order to compensate for user and coupling effects on the antenna performance. During this project we focused mainly on investigating MIMO capacity performance for the different prototypes and user scenarios. From the results, the highest capacity improvements are achieved when the PIFA is at the center. In addition for the talk mode scenario, we have achieved the highest improvement in capacity from adaptive matching (27% at the center frequency).

In terms of absolute capacity, the first and second prototypes have the highest capacity in most of the user scenarios. Moreover, Prototype II has a larger bandwidth as compared to the first prototype. On the other hand, Prototype III has the lowest capacity gain and absolute capacity in most of the cases. Nevertheless, this prototype has the largest bandwidth.

Therefore, if we only aim for the high capacity gain at the center frequency, the first prototype is the right choice. Nevertheless, it is impractical to employ this prototype since it does not cover the desired bandwidth. The second prototype can be the most promising prototype, since it has high capacity gains, with the highest improvement of 22 % in the case of data mode. In addition, it also has high absolute capacities and covers more than half of the desired bandwidth.

Prototype III, on the other hand has the largest bandwidth and is more robust than the other prototypes to hand interaction. The drawbacks are the low absolute capacities and high correlation.

Impedance Matching Results

A.1 Prototype I

A.1.1 Free space

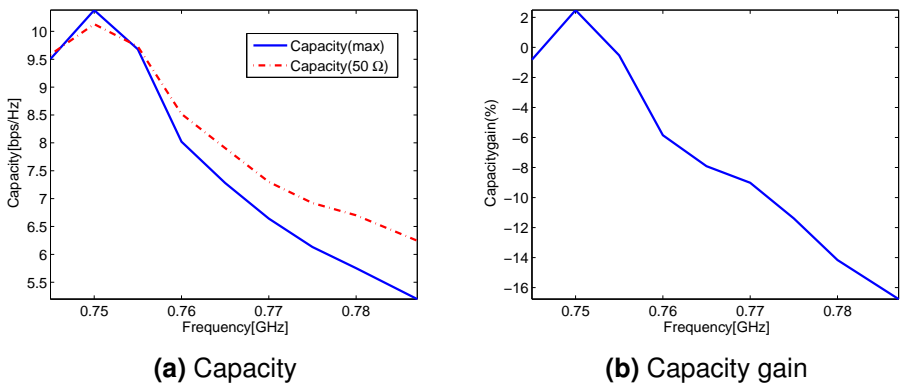
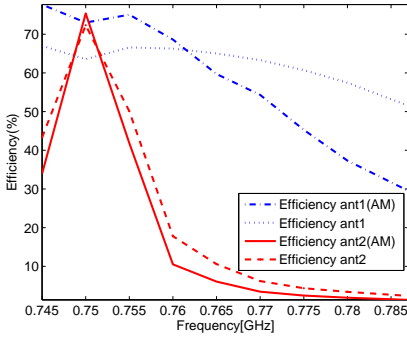
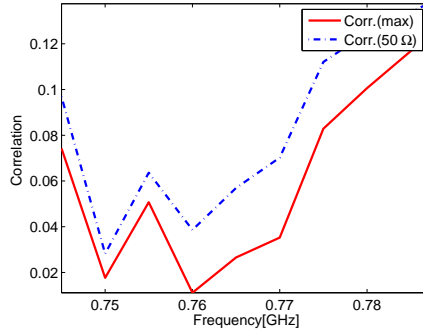


Figure A.1: Capacity for Prototype I in free space



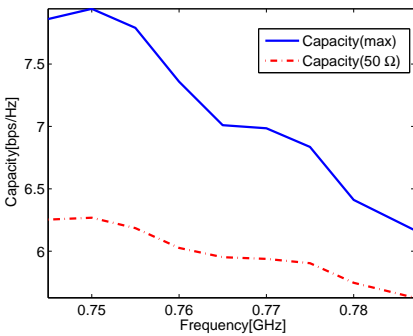
(a) Efficiency



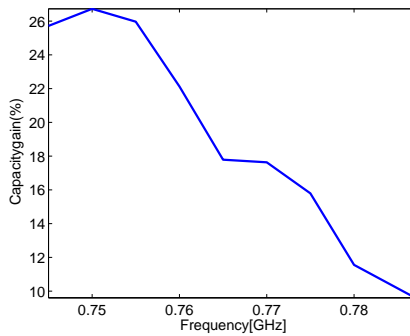
(b) Correlation

Figure A.2: Efficiency and correlation of Prototype I in free space

A.1.2 One hand data mode



(a) Capacity



(b) Capacity gain

Figure A.3: Capacity for Prototype I in data mode

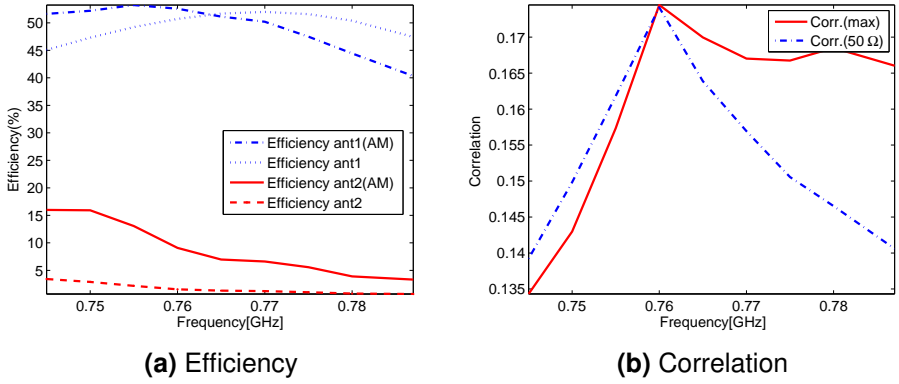


Figure A.4: Efficiency and correlation of Prototype I in data mode

A.1.3 One hand talk mode

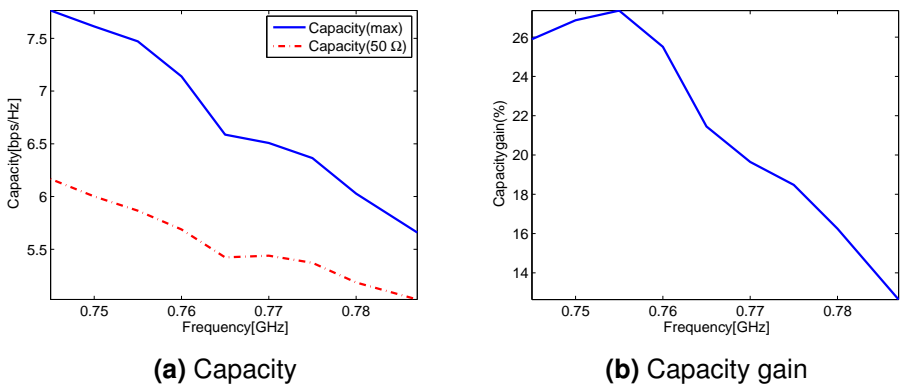
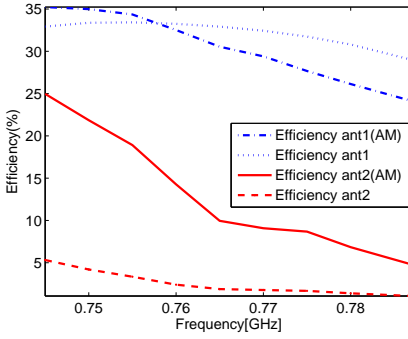
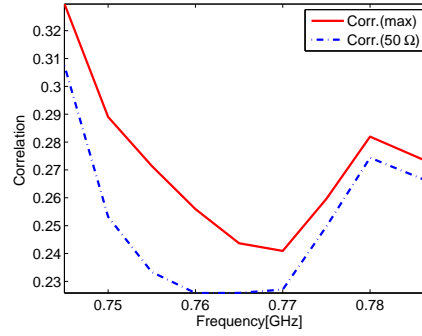


Figure A.5: Capacity for Prototype I in talk mode



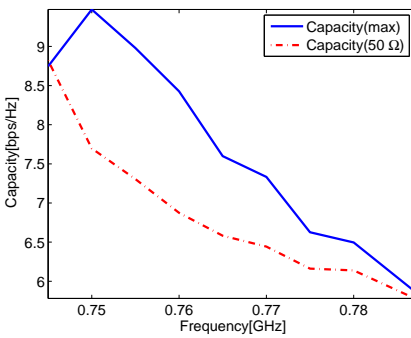
(a) Efficiency



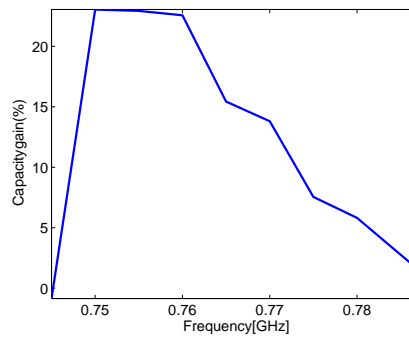
(b) Correlation

Figure A.6: Efficiency and correlation of Prototype I in talk mode

A.1.4 Two hands



(a) Capacity



(b) Capacity gain

Figure A.7: Capacity for Prototype I in game mode

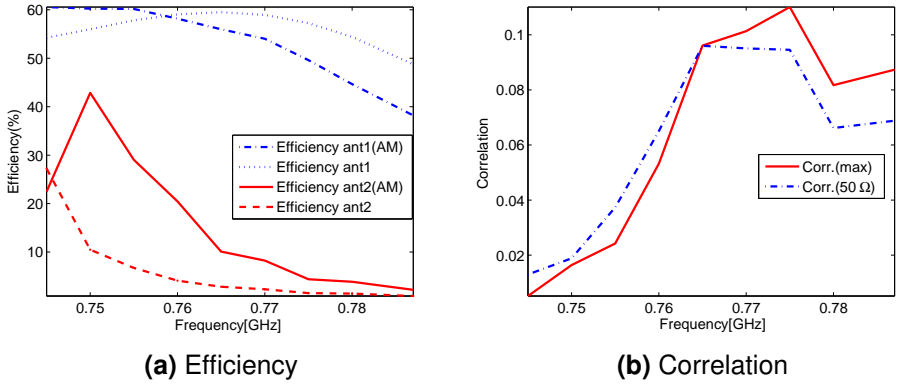


Figure A.8: Efficiency and correlation of Prototype I in game mode

A.2 Prototype II

A.2.1 Free space

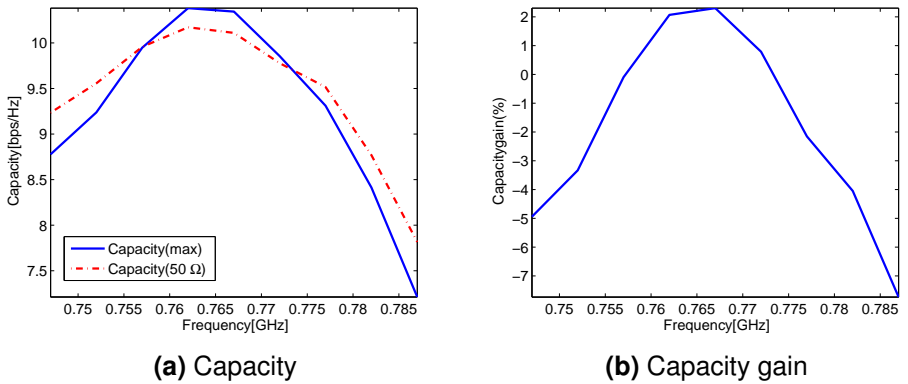
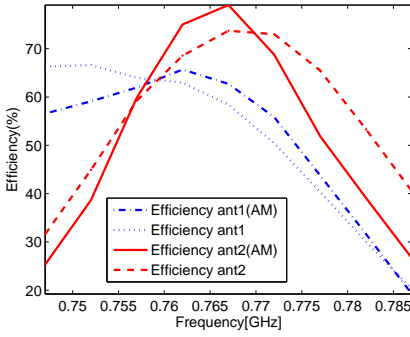
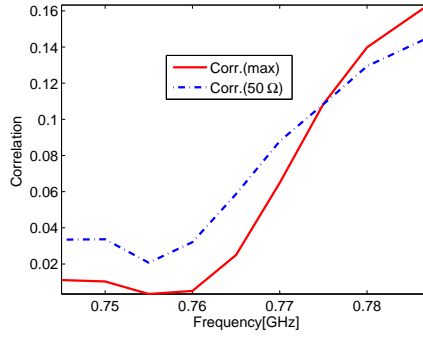


Figure A.9: Capacity for Prototype II in free space



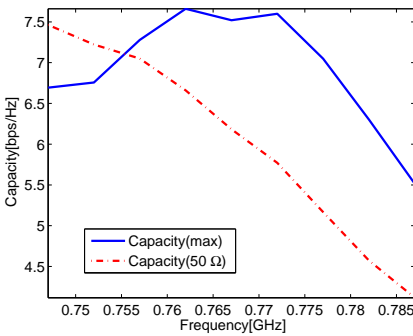
(a) Efficiency



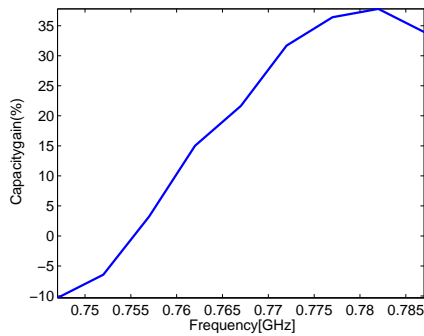
(b) Correlation

Figure A.10: Efficiency and correlation of Prototype II in free space

A.2.2 One hand data mode



(a) Capacity



(b) Capacity gain

Figure A.11: Capacity for Prototype II in data mode

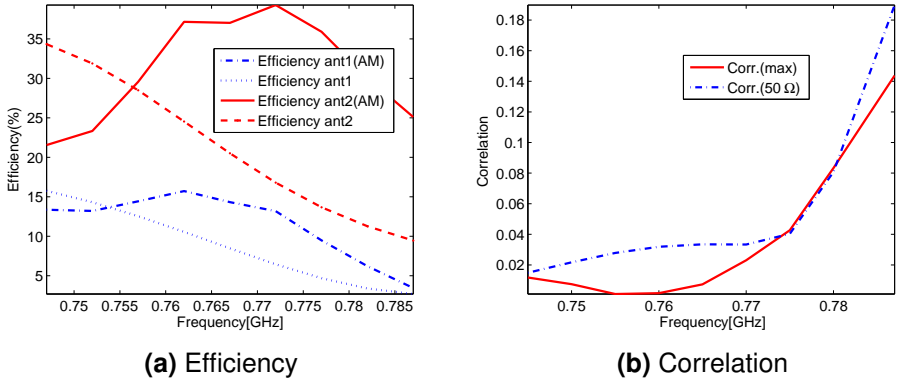


Figure A.12: Efficiency and correlation of Prototype II in data mode

A.2.3 One hand talk mode

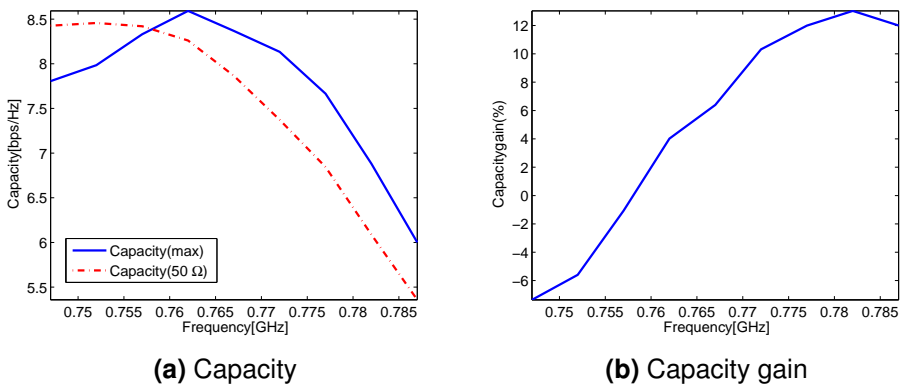
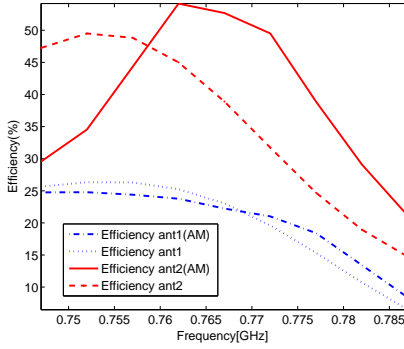
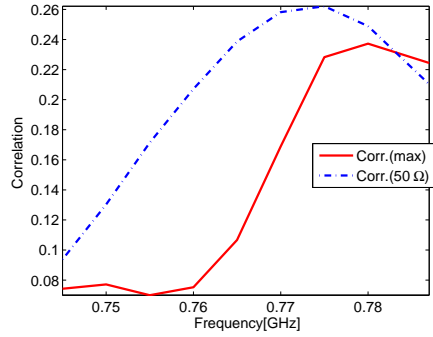


Figure A.13: Capacity for Prototype II in talk mode



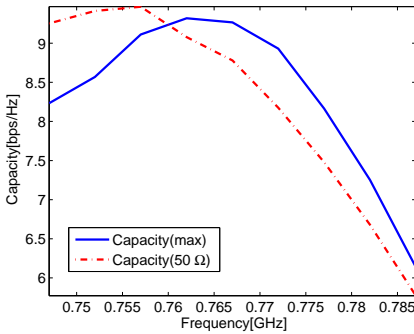
(a) Efficiency



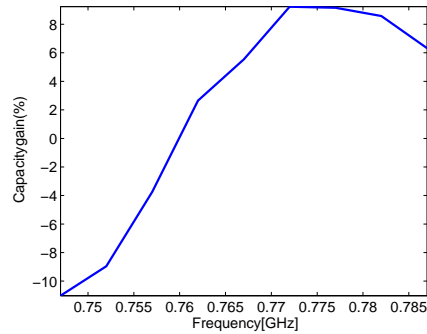
(b) Correlation

Figure A.14: Efficiency and correlation of Prototype II in talk mode

A.2.4 Two hands



(a) Capacity



(b) Capacity gain

Figure A.15: Capacity for Prototype II in game mode

A.3 Prototype III

A.3.1 Free space

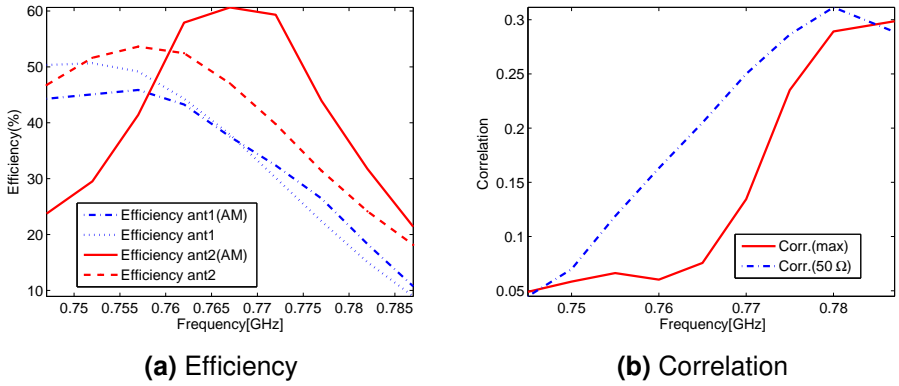


Figure A.16: Efficiency and correlation of Prototype II in game mode

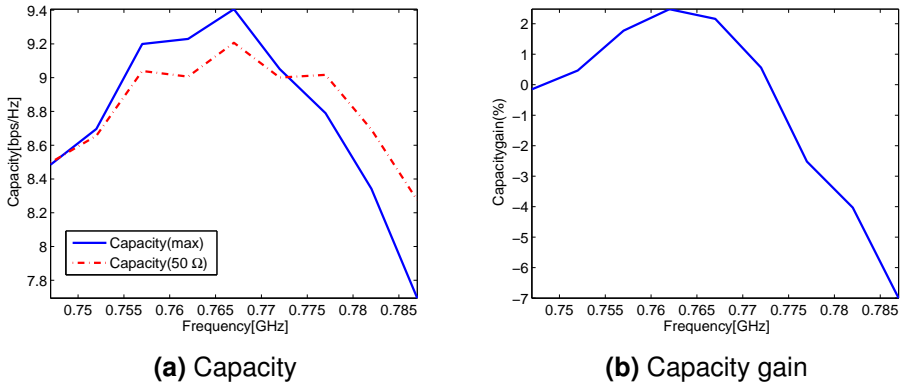


Figure A.17: Capacity for Prototype III in free space

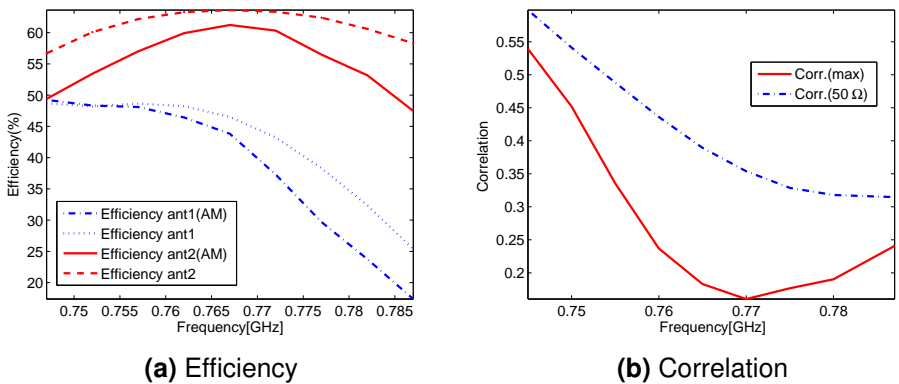
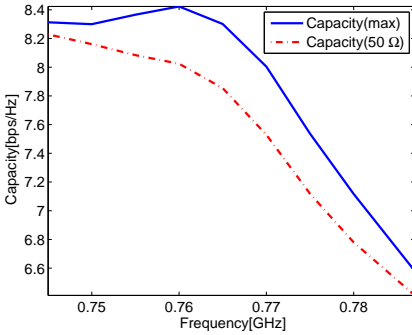
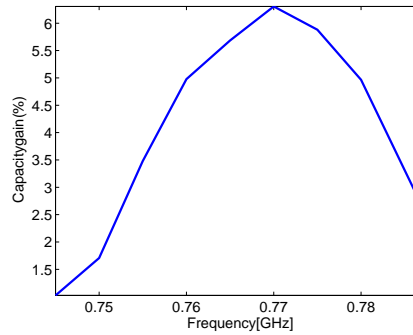


Figure A.18: Efficiency and correlation of Prototype III in free space

A.3.2 One hand data mode

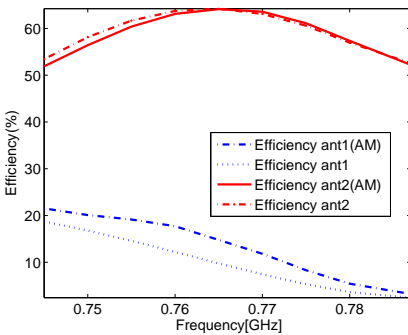


(a) Capacity

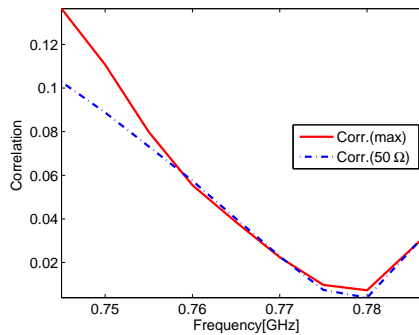


(b) Capacity gain

Figure A.19: Capacity for Prototype III in data mode



(a) Efficiency



(b) Correlation

Figure A.20: Efficiency and correlation of Prototype III in data mode

A.3.3 One hand talk mode

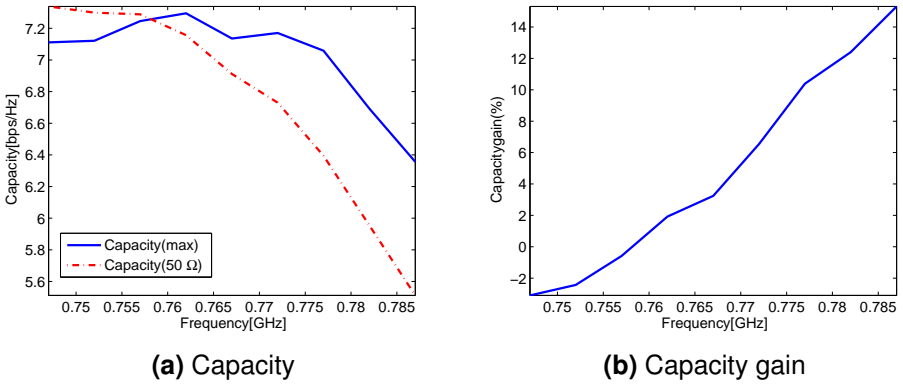


Figure A.21: Capacity for Prototype III in talk mode

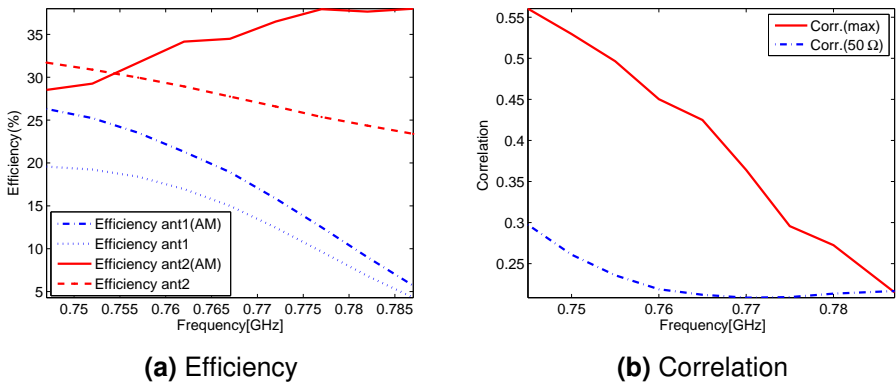
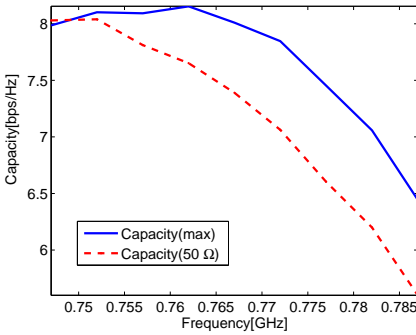
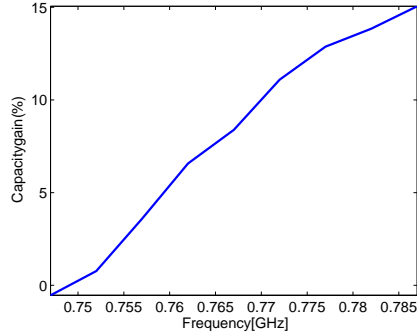


Figure A.22: Efficiency and correlation of Prototype III in talk mode

A.3.4 Two hands

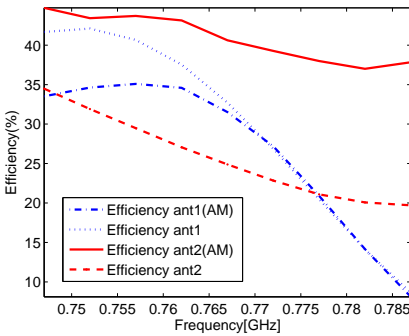


(a) Capacity

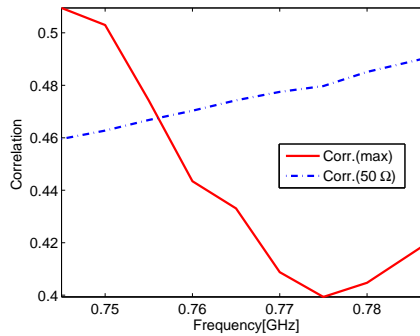


(b) Capacity gain

Figure A.23: Capacity for Prototype III in game mode



(a) Efficiency



(b) Correlation

Figure A.24: Efficiency and correlation of Prototype III in game mode

References

- [1] H. Li, Y. Tan, B. K. Lau, Z. Ying and S. He, "Characteristic mode based tradeoff analysis of antenna-chassis interactions for multiple antenna terminals," *IEEE Transactions on Antennas and Propagation*, vol. 60, no. 2, pp. 490-502, Feb. 2012.
- [2] C. Lin, K. Wong and S. Yeh, "Printed monopole slot antenna for multi-band operation in the mobile phone," *IEEE Transactions on Antennas and Propagation*, vol. 55, no. 12, pp. 629-632, Jun. 2007.
- [3] B. K. Lau, "Multiple antenna terminals," in *MIMO: From Theory to Implementation*, C. Oestges, A. Sibille, and A. Zanella, Eds. San Diego: Academic Press, 2011, pp. 267-298.
- [4] M. Pelosi, O. Franek, M. B. Knudsen, M. Christensen and G. F. Pedersen, "A grip study for talk and data modes in mobile phones," *IEEE Transactions on Antennas and Propagation*, vol. 57, no. 4, pp. 856-865, April 2009.
- [5] H. Wang and M. Zheng, "Input impedance-tuning slots of PIFA antennas," in Proc. *European Conference on Antennas and Propagation (EuCAP)*, 11-16 Nov. 2007.
- [6] B. K. Lau, J. B. Andersen, A. F. Molisch and G. Kristensson, "Antenna matching for capacity maximization in compact MIMO systems," in Proc. *International Symposium Wireless Communication Systems (ISWCS)*, pp. 253-257, 6-8 Sep. 2006.
- [7] C. A. Balanis, *Antenna Theory : Analysis and Design*, pp. 60-63, John Wiley & Sons, Inc., 1997.
- [8] http://niviuk.free.fr/lte_band.php.

- [9] V. Plicanic, "Antenna diversity studies and evaluation," Master thesis, Lund university, Lund, Sweden, May 2004.
- [10] S. Blanch, J. Romeu and I. Corbella, "Exact representation of antenna system diversity performance from input parameter description," *Electronic Letters*, vol. 39, no. 9, pp. 705-707, May 2003.
- [11] G. F. Pedersen, "Phantoms for radiation measurements of mobile phones," in Proc. *IEEE International Symposium on Personal Indoor and Mobile Radio Communications*, vol. 1, pp. C-95-C-99, Sep. 2001.
- [12] V. Plicanic, I. Vasilev, R. Tian and B. K. Lau, "Capacity maximisation of handheld MIMO terminal with adaptive matching in indoor environment," *Electronics Letters*, vol. 47, no. 16, pp. 900-901, Aug. 4 2011
- [13] K. Karlsson, "Embedded element patterns in combination with circuit simulations for multi-port antenna analysis," PhD dissertation, Chalmers University of technology, Gotenborg, Sweden 2009.
- [14] M. Jankiraman, *Space-time Codes and MIMO Systems*, Artech house, 2004.
- [15] A. Paulraj, R. Nabar and D. Gore, *Introduction to Space-Time Wireless Communications*, Cambridge, U.K.: Cambridge Univ. Press, 2003.
- [16] R. Tian, B. K. Lau and Z. Ying, "Multiplexing efficiency of MIMO antennas," *IEEE Antennas and Wireless Propagation Letters*, vol. 10, no., pp. 183-186, 2011.